Regional trends in the fractional solubility of Fe and other metals North Atlantic aerosols (GEOTRACES cruises GA01 and GA03) following a two-stage leach

Rachel U. Shelley[1, 2, 3], William M. Landing[1], Simon J. Ussher[2], Helene Planquette[3], and Geraldine Sarthou[3]

[1]Dept. Earth, Ocean and Atmospheric Science, Florida State University, 117 N Woodward Ave, Tallahassee, Florida, 32301, USA
[2]School of Geography, Earth and Environmental Sciences, University of Plymouth, Drake Circus, Plymouth, PL4 8AA, UK
[3]Laboratoire des Sciences de l'Environnement Marin, UMR 6539 LEMAR (CNRS/UBO/IRD/IFREMER), Institut Universitaire Européen de la Mer, Technopôle Brest-Iroise, Plouzané 29280, France

Correspondence to: Rachel U. Shelley (rshelley@fsu.edu)

Abstract. The fractional solubility of aerosol-derived trace elements deposited to the ocean surface is a key parameter of many marine biogeochemical models. Yet, it is currently poorly constrained, in part due to the complex interplay between the various processes that govern the solubilisation of aerosol trace elements. In this study, we used a sequential two-stage leach to investigate the regional variability in fractional solubility of a suite of aerosol trace elements (Al, Ti, Fe, Mn, Co, Ni, Cu, Zn, Cd and Pb) from samples collected during three GEOTRACES cruises to the North Atlantic Ocean (GA01, GA03-2010 and GA03-2011). We present aerosol trace element solubility data from two sequential leaches that provide a "solubility window", covering a conservative, lower limit to an upper limit, the maximum potentially soluble fraction, and discuss why this upper limit of solubility could be used as a proxy for the bioavailable fraction in some regions.

Regardless of the leaching solution used in this study (mild versus strong leach), the most heavily loaded samples generally had the lowest solubility. However, there were exceptions. Manganese fractional solubility was relatively uniform across the full range of atmospheric loading (32 ± 13 % and 49 ± 13 % for ultra-high purity water and 25 % acetic acid leaches, respectively). This is consistent with other marine aerosol studies. Zinc and Cd fractional solubility also appeared to be independent of atmospheric loading. Although the average fractional solubilities of Zn and Cd (Zn: 37 ± 28 % and 55 ± 30 %, Cd: 39 ± 23 % and 58 ± 26 % for ultra-high purity water and 25 % acetic acid leaches, respectively) were similar to Mn, the range was greater, with several samples being 100% soluble after the second leach. Finally, as the objective of this study was to investigate the regional variability in TE solubility, the samples were grouped according to air mass back trajectories (AMBTs). However, we conclude that AMBTs are not sufficiently discriminating to identify the aerosol sources or the potential effects of atmospheric processing on the physico-chemical composition and solubility of the aerosols.

1. Introduction

Aerosol trace element (TE) solubility is a key parameter of many biogeochemical models, but it is poorly constrained, e.g. Fe solubility estimates range from 0.001-90 % (Aguilar-Islas et al., 2010; Baker et al., 2016). The fractional solubility (herein referred to as "solubility") of aerosol TEs is defined in terms of the amount of a TE in solution from any given leach that passes through a filter (usually < 0.45 or 0.2 µm), expressed as a percentage of the total (Baker and Croot, 2010; Baker et al., 2016; Jickells et al., 2016). While this operational definition accounts for some of the variability in published values, it does not account for all of it. A number of factors impact aerosol TE solubility, such as: (1) the choice of leaching protocol, and (2) the aerosol source, which in turn is impacted by a combination of factors such as the mineralogy of the particles, atmospheric processing during transport, and the presence/absence of emissions from e.g. vehicles, industry and agricultural practices. Several studies have concluded that the most significant effects on aerosol Fe solubility result from the source/composition of the aerosols, rather than changes in physico-chemical parameters, such as temperature, pH and oxygen concentration of the leach medium, or the choice of batch versus flow-through techniques (e.g. Aguilar-Islas et al., 2010; Fishwick et al., 2014).

There have been a number of studies that have focused on the role of aerosol TEs on biogeochemical cycles in the North Atlantic (e.g. Sarthou et al., 2003; Baker et al., 2013; Buck et al., 2010; Ussher et al., 2013; Powell et al., 2015). More recently, the GEOTRACES programme has produced a number of aerosol datasets, which has stimulated further discussion on the use of this data to look for trends that link TE solubility and aerosol source (e.g. Baker et al., 2016; Jickells et al., 2016). Elemental ratios, enrichment factors and air mass back trajectory simulations have long been used as a first approximation of aerosol source, and there are many studies that employ multivariate statistical analyses for aerosol source apportionment (e.g. Chueinta et al., 2000; Laing et al., 2015). In addition, more studies are making use of stable isotope ratios to investigate aerosol provenance. Some of these methods are well-established and have a relatively long history of use in this purpose, such as Pb isotopes (e.g. Maring et al., 1987), and Sr and Nd isotopes (e.g. Skonieczny et al., 2011; Scheuvens et al., 2013 and references therein), and data from investigations of novel isotope systems are increasing. For example, Fe isotopes show promise as a way to differentiate between anthropogenic and mineral dust aerosols (Conway et al., submitted). In contrast, Cd isotopes may not be a suitable tool for aerosol source apportionment (Bridgestock et al., 2017).

As the soluble fractions of aerosol TEs are thought to be the most-readily bioavailable forms (Shaked and Lis, 2009), the leachable (soluble) fraction is used as a first approximation of the bioavailable fraction. Therefore, experimental conditions should mimic natural conditions as closely as possible, while yielding reproducible results. Ideally, the leach protocol used fits both these criteria. However, that is not always strictly possible for reasons such as access to the leach medium of choice,

availability of analytical instrumentation, and cost. Currently, however, there is no standardised aerosol leaching protocol, but it is recognised that this should be a priority for future studies (Baker et al., 2016). Some commonly-used leach media are ultra-high purity (UHP) water (18.2 MΩ.cm), seawater, weak acids (e.g. 1% HCl, 25 % acetic acid), or ammonium acetate buffer (e.g. Buck et al., 2006, Baker et al., 2006b; Berger et al., 2008).

To investigate the regional variation in the solubility of key TEs in the North Atlantic, aerosol samples were collected during the US-GEOTRACES GA03 campaigns in 2010 and 2011, and the French GEOTRACES GA01 campaign in 2014 (www.geotraces.org). The focus of this paper is Fe and the GEOTRACES "key" trace elements, Al, Cd, Cu, Mn, Pb, Zn, plus Co, Ni, and Ti (GEOTRACES Planning Group, 2006). This suite of TEs includes bioactive elements, tracers of atmospheric deposition, and elements characteristic of anthropogenic aerosols. Some TEs fit into more than one of these categories. Here, we use the term 'trace element' in the context of open ocean water column concentrations, thus acknowledging that elements such as Al, Fe and Ti are not present in trace concentrations in aerosol source material. Aerosol concentrations for a suite of other elements (Li, Na, Mg, P, Sc, V, As, Se, Rb, Sr, Sn, Sb, Cs, Ba, La, Ce, Nd, Th, U) were also determined, but will not be discussed further here. However, these data are available at BCO-DMO (GA03; www.bco-dmo.org/) and LEFE-CYBER (GA01; (www.obsvlfr.fr/proof/php/GEOVIDE/GEOVIDE.php), and on request from the lead author.

In this study a two-stage leach protocol was followed. the first leach employed was the "instantaneous" leach described by Buck et al. (2006) which is a flow-through method where the leach medium is in contact with the aerosols for 10 - 30 s. It can be conducted using UHP water or seawater. The advantages of using UHP water are that UHP water is a reproducible medium (allowing for inter-lab comparisons) that can easily be analysed by ICP-MS for many elements simultaneously without the need for time-consuming sample handling steps such as separation techniques and drying down then re-dissolving the residue. Leaches with UHP water can be conducted at sea, or in the home laboratory. If fresh sea water is used the leaches must be undertaken at sea.

Given that UHP water and rain water have broadly similar pH (~ pH 5.6), UHP water is used as an analogue for rain/wet deposition, as wet deposition is thought to dominate the supply of many TEs, at least at some regional and local scales (Helmers and Shremms, 1995; Kim et al., 1999; Powell et al., 2015). However, the extremely low ionic strength of UHP water, and the absence of the metal binding ligands naturally present in rain water and seawater (e.g. Chieze et al., 2012; Wozniak et al., 2014), means that UHP water is not a perfect analogue for oceanic receiving waters. As such, freshly-collected, filtered ($< 0.2 \mu$m) seawater likely produces a better estimate of the fractional solubility of TEs on first contact with oceanic receiving waters. For Fe, leaches using UHP water (~ pH 5.6)

109 typically produce higher solubility estimates than leaches conducted with natural seawater (~ pH 8.2)

110 due to the pH sensitivity of dissolution and the higher ionic strength of sea water. On occasions where

111 higher solubility in seawater is observed, complexation by Fe binding ligands is likely the cause.

112 Regardless of whether UHP water or seawater is used, the instantaneous leach likely yields

113 conservative lower limit estimates of TE solubility due to the short contact time between the aerosols

114 and leach medium, and reports that aerosol solubility has a bi-modal behaviour for many TEs (initial

115 fast release, followed by a slower sustained release with time; e.g. Desboeufs et al. 2005; Kocak et al.,

116 2007; Mackey et al., 2015).

117 The second, sequential leach was employed in order to estimate an upper limit of TE solubility, and

118 provide a "solubility window", but also as an estimate of the maximum bioavailable fraction during

119 the residence time of aerosol particles in the euphotic zone. We used the 25 % acetic acid leach with

120 hydroxylamine hydrochloride described by Berger et al. (2008). The pH of this leach (pH 2.1) is just

121 below that of zooplankton or fish digestive tracts and the reducing agent mimics the low oxygen

122 environments inside faecal pellets and marine snow aggregates. Indeed, Schmidt et al. (2016) have

123 demonstrated that lithogenic Fe is mobilised in the gut passage of krill resulting in threefold higher Fe

124 content in the muscle, and fivefold higher Fe content of the faecal pellets of specimens close to

125 lithogenic source material compared to those from offshore.

126 **2. Methods**

127 **2.1. Aerosol sample collection**

128 Aerosol samples (n = 57) were collected aboard the *R/V Knorr* during the *US-GEOTRACES GA03*

129 cruises (15 Oct – 2 Nov 2010 and 6 Nov – 9 Dec 2011, and aboard the *N/O Pourquoi Pas?* during the

130 French GEOTRACES GA01 cruise (GEOVIDE, 15 May – 30 June 2014) (Fig. 1). Both campaigns

131 took place in the North Atlantic Ocean, with GA03-2010 and GA01 departing from Lisbon, Portugal.

132 The cruise tracks were designed to traverse a wide variety of biogeochemical provinces (Longhurst,

133 2010) including; continental shelf regions, an eastern boundary current upwelling system (off West

134 Africa), the oligotrophic North Atlantic gyre, and sub-Arctic waters, and to span a large gradient in

135 atmospheric dust loading. The aerosol collections have been described previously (Wozniak et al.,

136 2013; 2014; Shelley et al., 2015; 2017). Briefly, air was simultaneously pulled through twelve acid-

137 washed 47 mm diameter Whatman 41 (W41) ashless filter discs at approximately 1.2 m^3 min^{-1} (134

138 cm s^{-1} face velocity) using a high-volume aerosol sampler (TSP model 5170V-BL, Tisch

139 Environmental). The metadata and concentration data for the aerosol leaches can be found in the

140 supplementary information (Table S1). All filters were stored frozen (-20°C) and double bagged prior

141 to processing, both on the ship and upon returning to the home laboratories.

142 To avoid contamination from the ship's stack exhaust, aerosol sampling was controlled with respect to

143 wind sector and wind speed using an anemometer interfaced with a datalogger (CR800, Campbell

144   Scientific). The samplers were programmed to run when the wind was ± 60° from the bow of the ship

145   and > 0.5 m s^{-1}. When the wind failed to meet these two criteria, the motors were shut off

146   automatically and not allowed to restart until the wind met both the speed and direction criteria for 5

147   continuous minutes. In addition, the samplers were deployed on the ship's flying bridge as high off the

148   water as possible (~14 m above sea level) to minimise collection of sea spray.

149

150 **2.2. Trace element determination – totals aerosol TEs**

151   The total digestion method of Morton et al. (2013) was used for the determination of total aerosol TE

152   loadings (Al, Ti, Mn, Fe, Co, Ni, Cu, Zn, Cd, Pb). The W41 filter discs were digested in tightly-

153   capped 15 mL Teflon-PFA vials (Savillex). Firstly, 1000 µL of ultrahigh purity (UHP) 15.8 M nitric

154   acid (Optima or Merck Ultrapur) was added to each vial, heated to 150 °C on a hotplate, and then

155   taken to dryness. Secondly, 500 µL of 15.8 M nitric acid (13.2 M HN0$_3$) and 100 µL of 28.9 M

156   hydrofluoric acid (5.8 M HF) (Optima or Merck Ultrapur) was added to each vial, re-heated to 150 °C

157   on a hotplate, then taken to near dryness. After the final digestion and evaporation step, the samples

158   were re-dissolved in 20 mL of 0.32 M nitric acid for analysis. All filter digestions were performed

159   under Class-100 laminar flow conditions. Total aerosol TE concentrations were determined by

160   magnetic sector field inductively coupled plasma mass spectrometry (ICP-MS; Thermo Element-2) at

161   the National High Magnetic Field Laboratory (NHMFL) at Florida State University (FSU; GA03) or

162   Pôle de Spectrométrie Océan (PSO) at the Institut Universitaire Européen de la Mer, France (IUEM;

163   GA01). Samples were introduced to a PFA-ST nebuliser (Elemental Scientific Inc.) via a modified

164   SC-Fast introduction system consisting of an SC-2 autosampler, a six-port valve and a vacuum rinsing

165   pump. Replicate blank solutions for the acid digestions were prepared by digesting W41 discs that had

166   been deployed in the aerosol samplers for 1 h while not in operation, and the resulting concentrations

167   were subtracted from all acid-digested filter samples. Details of the digestion blanks and analytical

168   figures of merit, including CRM recoveries, have previously been reported (Shelley et al., 2015;

169   2017).

170

171 **2.3. Trace element determination – soluble aerosol TEs**

172   In this study, we used a two-step, sequential leach to investigate regional variation in aerosol sources,

173   TE fractional solubility and bioavailability. We discuss the results from (1) an 'instantaneous' leach

174   (Buck et al., 2006), that provides a lower limit estimate of the most labile TE fraction (analogous to

175   the initial rapid release of TEs into rain drops and the surface mixed layer of the ocean), followed by

176   (2) a more protracted leach using 25 % acetic acid (with the reducing agent, hydroxylamine

177   hydrochloride, and heat, 10 min at 90 °C), which mimics the slower and sustained release from aerosol

178   particles during their residence time in the euphotic zone.

179   The first step, the "instantaneous" leach, was conducted under a Class-100 laminar flow hood. In this

180   technique, 100 mL of UHP water (> 18 MΩ•cm resistivity, pH ~ 5.5, Barnstead Nanopure) is rapidly

181   passed through an aerosol-laden W41 filter held in a polysulfone vacuum filtration assembly

182   (Nalgene). Operationally-defined dissolved (≤ 0.45 µm) TEs are collected in the filtrate (leachate) by

183   positioning a GN-6 Metricel backing filter (cellulose esters) below the W41 disc in the filtration

184   assembly (Buck et al., 2006). In this study, the leachate was transferred to an acid-clean low density

185   polyethylene (LDPE) bottle and acidified to 0.024 M (~ pH 1.7) with UHP HCl and double-bagged for

186   storage until analysis at FSU or IUEM. As for total elemental determinations, soluble TEs in the

187   leachate were also determined by ICP-MS. Leachate blanks were prepared by passing 100 mL of UHP

188   water through W41 filters that had been deployed in the aerosol sampler for 1 h while not in operation.

189   For example, leachate blanks for Fe represented an average of 1.6 ± 0.4 % and 15.5 ± 15.8 % of the Fe

190   sample concentrations for GA03 and GA01, respectively). A subset of samples (GA03-2011) were

191   also leached using the instantaneous leach procedure with freshly collected, filtered (0.2 µm) seawater

192   as the leach medium. Leachate blanks were subtracted from all leachate sample concentrations, details

193   of which can be found in Table S1 in the Supplementary Material.

194

195   The UHP water fractional solubility was calculated using Eq. (1):

196 $$\frac{[element]_{UHP\ water\ leach}}{[element]_{total}} * 100 = UHP\ water\ Fractional\ Solubility$$

197   (1)

198   Following the instantaneous UHP water leach, the filter was transferred to a 15 mL centrifuge tube,

199   and the second leach was undertaken, using 5 mL of 25 % (4.4 M) ultrapure acetic acid, with 0.02 M

200   hydroxylamine hydrochloride as the reducing agent (Berger et al., 2008). After a 10 min heating step

201   (90 °C), the leaches were left for 24 h before being centrifuged for 5 min at 3400xg. The leachate was

202   then carefully decanted into acid-clean LDPE bottles. In order to rinse any residual acetic acid from

203   the filter, 5 mL of UHP water was pipetted into the centrifuge tubes, which were then centrifuged

204   again for 5 min at 3400xg. This supernatant was then added to the acetic acid leachate in the LDPE

205   sample bottles. As this second leach aims to access a less labile fraction of the TEs of interest

206   (including TEs absorbed to surfaces, TE oxyhydroxides and TEs complexed by aerosol organic

207   matter), without significantly attacking TEs bound within the mineral matrix (Koçak et al., 2007;

208   Berger et al., 2008), it may provide an upper limit estimate for the fractional solubility of these aerosol

209   TEs as the aerosols mix down into the ocean. There is a slight risk that the heating step could begin to

210   attack the mineral matrix, resulting in a slight over-estimation of the upper limit of solubility, but this

211   risk was shown to be minimal (Berger et al., 2008). Despite this risk, the heating step was included

212   because of the desire for procedural similarity with marine particle leaches from the same cruises (e.g.

213   Planquette et al., 2016; H. Planquette and A. Gourain pers. comm.), which have been used to assess

214 the relative importance of atmospheric inputs of TEs to water column concentrations of Al, Fe and Pb

215 (Menzel-Baraqueta et al.; Tonnard et al.; Zurbrick et al., this issue).

216 As all samples in this study were leached first using the UHP water instantaneous leach, followed by a

217 sequential leach with 25 % acetic acid, the overall solubility in 25% acetic acid was calculated using

218 Eq. (2):

219 $$\frac{[element]_{UHP\ water\ leach}}{[element]_{total}} + \frac{[element]_{25\ \%\ HAc\ leach}}{[element]_{total}} * 100 = HAc\ Fractional\ Solubility$$

220 (2)

221 **2.4. Major anion determination**
222 Before the UHP water leachate was acidified, a 10 mL aliquot was taken from each leach sample for

223 the determination of the soluble major anions. The aliquot was immediately frozen for storage. The

224 anions, Cl^-, NO_3^- and SO_4^{2-}, were determined by ion chromatography using either a Dionex 4500i (at

225 FSU for GA03 samples) or a Metrohm, IC850 system (at Laboratoire Interunivesitaire des Systèmes

226 Atmosphériques, Paris for GA01 samples).

227

228 **2.5. Air mass back trajectory simulations**
229 Air mass back trajectory (AMBT) simulations were generated using the publicly-available NOAA Air

230 Resources Laboratory Hybrid Single-Particle Lagrangian Integrated Trajectory (HYSPLIT) model,

231 using the GDAS meteorology (Stein et al., 2015; Rolph, 2017). The 5-day AMBT simulations were

232 used to describe five regional categories, based on the predominant trajectories for the air masses. The

233 simulations and further details of these categories can be found in Wozniak et al., (2013; 2014) and

234 Shelley et al., (2015; 2017). Briefly, for cruise GA03 air masses were characterised as European,

235 North American, North African, or Marine (no or minimal interaction with major continental land

236 masses within the 5-day simulation period). For cruise GA01, all the samples were classified as High

237 Latitude dust (originating north of 50°N; Bullard et al., 2016). The classifications are shown in Table

238 S1, and the AMBT simulations from Shelley et al. (2015; 2017) have been reproduced and can be

239 found in the Supplementary Material (Fig. S1). The simulations use arrival heights of 50, 500 and

240 1500 m, so that at least one height was located in the marine boundary layer.

241

242 **3. Results and Discussion**
243 **3.1. Identifying aerosol provenance**
244 Air mass back trajectory (AMBT) simulations are frequently used to identify the origin and/or flow

245 path of air masses, from which a first approximation of aerosol provenance (e.g. deserts, urban

246 regions, or biomass burning) are made. While a useful tool in oceanographic studies, AMBTs used

247 alone do have limitations. Perhaps the most significant of these is that they are unable to quantify the
248 contribution of different aerosol types or the entrainment of particles along the flow path of the air
249 mass. Indeed, within the five categories described in this study multiple sources are likely to have
250 contributed to the composition of the bulk aerosol of each category. This study is likely to be
251 particularly sensitive to this as the sampling site was not static (i.e. sampling occurred along three
252 different transects), and air masses can, and do, take different pathways within a general wind
253 direction. Consequently, AMBTs are not adequately discriminating for aerosol source apportionment.
254 However, we have organised the data using the AMBT categories as the objective of this study was to
255 look for trends in solubility at a regional level, and also for consistency with our earlier published
256 work from the North Atlantic (Wozniak et al., 2013; 2014; Shelley et al., 2015; 2017).

257 More powerful approaches for aerosol source apportionment consider the physico-chemical
258 composition of the aerosols, either as the bulk aerosol or individual particles. There have been a
259 number of field campaigns (e.g. DABEX, DODO, SAMUM and AMMA) and individual studies
260 which have provided a wealth of information about the physico-chemical composition of African dust
261 before, during and after long-range transport (e.g. Johansen et al., 2000; Johnson et al., 2008;
262 McConnell et al., 2008; Petzold et al., 2009; Marticorena et al., 2010; Trapp et al., 2010; Formenti et
263 al., 2011). These studies, and satellite data have identified the key dust source regions in North Africa
264 (Prospero et al., 2002). Chemical composition data for other aerosol end members which supply
265 aerosols to the North Atlantic is not as extensive, but some examples of individual studies and field
266 campaigns can be found in Table S2. In addition, campaigns in the Atlantic Ocean which have
267 sampled marine aerosols (e.g. Atlantic Meridional Transect, CLIVAR, GEOTRACES) have identified
268 aerosol sources from characteristic groups of elements and elemental ratios (e.g. high concentrations
269 of lithogenic elements are characteristic of a mineral dust, K is a tracer of biomass burning, and
270 correlations between V and Ni are diagnostic of emissions from marine shipping; Baker et al., 2006a;
271 Sippula et al., 2014; Baker and Jickells, 2017), organic compounds (e.g. Wozniak et al., 2013; 2014,
272 2015), and/or stable isotopic signatures (Scheuvens et al., 2013 and references therein).

273 Although atmospheric inputs to the ocean are episodic and exhibit a seasonality in the tropical and
274 subtropical North Atlantic that is largely driven by the migration of the intertropical convergence zone
275 (Prospero et al., 1981; Adams et al., 2012; Doherty et al., 2014), North African/Saharan mineral dust
276 dominated the aerosol composition in the GA03 study region (Conway and John, 2014; Shelley et al.,
277 2015; Conway et al., submitted). Other aerosol sources in Europe and North America and sea salt also
278 contributed to the bulk aerosol to varying extents. In contrast to GA03, the GA01 transect was located
279 north of the extent of the Saharan dust plume (~ 25° N in summer, Ben-Ami et al., 2009), and was
280 thus influenced by a mixture of high latitude dust sources (Prospero et al., 2012; Shelley et al., 2017),
281 which also have a seasonal cycle. As a result, a large dynamic range of aerosol loading was observed

282 (Fe = 0.185–5650 ng m^{-3}; Al = 0.761- 7490 ng m^{-3}) during these two campaigns, with the highest Fe

283 and Al loadings associated with the North African samples (GA03), lower loadings with the Marine

284 samples (GA03), and the lowest loadings observed in the samples collected in the Labrador Sea

285 (GA01).

286 Total Fe and Al were strongly correlated (r^2 = 0.999, Pearson's ρ P < 0.01), demonstrating that the two

287 metals have common lithogenic source(s) (Fig. 2). However, this correlation was largely driven by the

288 heavily-loaded North African samples (r^2 = 0.997, P < 0.01). For each of the other source categories,

289 simple linear regression of the data resulted in r^2 values of: 0.879 (P < 0.01) for High Latitude dust

290 (GA01), 0.890 (P = 0.057) for European samples (GA03), 0.983 (P = 0.34) for N. American samples

291 (GA03) and 0.751 (P = 0.70) for Marine samples (GA03) (Fig. 2b). Further discussion of sub-regional

292 differences in the Fe/Al ratio are addressed later in the Discussion. For the other TEs, strong

293 correlations for the combined GA01 and GA03 datasets were found between Ti/Al (r^2 = 0.999, P <

294 0.01), Mn/Al (r^2 = 0.994, P < 0.01) and Co/Al (r^2 = 0.996, P < 0.01), in accord with previous

295 observations in this region owing to the primarily lithogenic sources of these elements (e.g. Jickells et

296 al., 2016). The correlations between Al and the primarily anthropogenic TEs, Ni, Cu, Zn, Cd, and Pb,

297 were also significant at the 99% confidence level : Ni/Al (r^2 = 0.884), Cu/Al (r^2 = 0.652), Pb/Al (r^2 =

298 0.478), Zn/Al (r^2 = 0.321), Cd/Al (r^2 = 0.303) due the presence of the heavily-loaded North African

299 samples, which accounted for between 88 % and 30 % of the statistical variance for Ni and Cd,

300 respectively. Sources other than mineral dust (e.g. metal smelting emissions, fly ash, vehicle

301 emissions, volcanic ash, proglacial till) are presumably responsible for the residual variance.

302 Establishing the contributions from these other aerosol sources and their influence on TE solubility is

303 a research priority.

304 As the aerosol source has a direct bearing on the type and composition of aerosols, determining the

305 source could provide useful data that might be used to predict the fractional solubility of aerosol TEs.

306 As positive matrix factorisation (PMF) can be used for source apportionment, we used the USA

307 Environmental Protection Agency's EPA PMF model (v. 5.0) with the total TE concentration data to

308 look for trends in the data. However, the GA01 and GA03 dataset is relatively small (n = 57) and the

309 model was not stable with more than two factors. The two factors were a mineral dust factor (high

310 contributions from lithogenic TEs, in particular Al, Ti, Fe and Zr) and a pollution/anthropogenic factor

311 (with high contributions from Zn and Pb) (Fig. S2a, Supplementary Material). As anticipated, the

312 mineral dust factor dominated where North African aerosols were sampled, and the pollution factor

313 was relatively more important closer to the European and North American continents (Fig. S2b). This

314 is in accord with the samples from North Africa having elemental mass ratios that are consistently the

315 closest to the UCC elemental ratios compared to aerosols from the other source regions (Fig. 3). In

316 the High Latitude samples, the pollution factor and the mineral dust factor were of approximately

equal dominance. Interestingly, the North African aerosols also contained a relatively strong pollution component, consistent with a northeast flow into North Africa from Europe, followed by entrainment of mineral dust during passage over the Sahara (Baker and Jickells, 2017). Given that the PMF indicates that 100 % of the variability in the Cd concentrations was explained by the pollution factor, this suggests that Cd in North African aerosols is not sourced from mineral dust, which would explain why no fractionation was observed in Cd isotopes from North African and European aerosols (Bridgestock et al., 2017). Further, it also suggests that even the relatively homogeneous aerosols from North Africa do not represent a 'pure' end-member. However, the PMF analysis was not sensitive enough to identify the full complement of aerosol sources contributing to the samples collected during GA01 and GA03.

3.2. Elemental mass ratios and aerosol source

Elemental mass ratios from the ten most heavily loaded GA03 North African aerosols were averaged to derive a value for the 'North African' ratio depicted by the dashed horizontal line in Figures 3(a-i). Aluminium was used to normalise the data (Fig. 3; Table S2) and was chosen instead of Ti, another proxy for mineral dust, due to the presence of some anomalously high Ti/Al ratios in some of the Marine samples during GA03 (Fig. 3a; Shelley et al., 2015). We have previously reported a mass ratio of 0.76 for Fe/Al for the North African end-member aerosols (Shelley et al., 2015; Fig. 2a), which is significantly higher than the mean upper continental crustal (UCC) ratio of 0.47 (Rudnick and Gao, 2003) but entirely consistent other studies of Saharan soils and dust (e.g. Chiapello et al., 1997; Guieu et al., 2002; Lafon et al., 2006; Baker et al., 2013).

For North African dust there does not appear to be a discernible source dependent trend in Fe/Al ratios due to a natural variability in Fe-bearing minerals in soils in dust source regions (Lafon et al., 2006; Scheuvens et al., 2013), but it might be possible to use Fe/Al ratios for some of the other aerosol groups to suggest different sources. For example, the European samples (n = 4) fall into two sub-groups: two samples have low Fe/Al ratios (Fig. 2; E3 = 0.48, E4 = 0.10 and Fig. 3c), whereas the other two samples (E1 = 0.95 and E2 = 0.78) have Fe/Al ratios within the range of the North American samples (Fe/Al 1.1 ± 0.22, range 0.86-1.42) and all but one of the Marine samples (Fe/Al, excluding M12, 0.93 ± 0.33, range 0.59-1.61; M12, collected closest to the North African samples, Fe/Al = 0.43).

Aerosols from the more northerly section, GA01, were largely outside the influence of the Saharan dust plume (Shelley et al., 2017), and are all classified as High Latitude in this study (Fig. 3). For this group of samples, there were also sub-groups of Fe/Al ratios. During the first half of the cruise (Fig. 1), there was a group of samples (G1-6, G8 and G10) with Fe/Al ratios of 0.58 ± 0.05; Fig.3c). This is intermediate between the UCC ratio (0.48 ± 0.07) and the North African mineral dust ratio (0.78 ±

351   0.03; Fig. 3c). For these samples, the wind direction was predominantly from the north/north west

352   (Shelley et al., 2017), so it is unlikely that the observed ratios reflect a mixture of North African

353   mineral dust and European aerosols. Rather, it more likely comes from high latitude sources, as dust

354   supplied by proglacial till from Iceland and Greenland peaks in spring/early summer, and can be

355   deposited over the Atlantic Ocean (Prospero et al., 2012; Bullard et al., 2016). Unfortunately, the

356   extensive cloud cover experienced during the GA01 cruise (May/June 2014) prevented the use of

357   satellite observations (e.g. http://worldview.earthdata.nasa.gov) which would have confirmed the

358   presence of dust from these sources. The elemental ratios calculated from TE concentrations from

359   volcanic ash sampled during the eruption of the Eyjafjallajökull volcano in 2010 (Achterberg et al.,

360   2013) offers some limited support for this argument, as our range of elemental ratios encompasses this

361   end-member (Icelandic soils are almost exclusively volcanic in origin; Arnalds 2004). However,

362   although Icelandic sands (Baratoux et al., 2011) and tephra (Oladottir et al., 2011) have Mn/Al ratios

363   that overlap the GA01 samples, Fe/Al is generally lower in our High Latitude dust samples (Table S2).

364   A second group of GA01 samples (G7, G9, G11 and G12) had Fe/Al ratios of 0.34 ± 0.01, but no

365   obvious link in terms of the AMBTs. The Greenland shelf and Labrador Sea samples, except G15, had

366   low Fe/Al (0.16 ± 0.04), and were distinct from those collected on the Canadian shelf (0.48 ± 0.02).

367   These trends strongly suggest that the High Latitude dust was made up of at least four aerosol sources.

368   While there is evidence for anthropogenic source(s) of aerosol Fe to the North Atlantic (Conway et al.,

369   submitted), which is more soluble than Fe associated with mineral dust (Sedwick et al., 2007;

370   Sholkovitz et al., 2009; 2012), North African mineral dust dominates the supply of Fe to much of the

371   study region (Baker et al., 2013; Shelley et al., 2015; 2017; Conway et al., submitted). In addition to

372   the samples classified as European and North American, elevated Fe/Al ratios were also observed in

373   the Marine samples (Fig. 2b). In addition to aerosols derived from continental sources (meaning either

374   mineral dust or anthropogenic emissions), sea spray aerosols could make a relatively higher

375   contribution to the bulk aerosol in remote oceanic locations (de Leeuw et al., 2014). However, this

376   would have the opposite effect as the ratio of Fe/Al in surface seawater ($0.017 - 0.024$ in the North

377   Atlantic gyre, 0.019 European continental shelf, and $0.030 - 0.031$ in the Mauritanian upwelling zone;

378   Hatta et al., 2015) is two orders of magnitude lower than the crustal ratio. Hence the contribution of

379   sea spray aerosols appears to have a negligible impact on the Fe/Al ratios in the bulk Marine aerosols.

380   The Marine, and the High Latitude samples had the widest range in Fe/Al ratios and were also

381   collected in the most remote locations. These groups also had the greatest difference in the Fe/Al

382   ratios between the total and soluble fractions, and also contained the samples with the lowest ratios of

383   Fe/Al in the soluble fraction (minimum Fe/Al = 0.15, samples G9-GA01 and M3-GA03; Fig. 3c),

384   suggesting that even though aerosol Fe is altered towards more soluble forms during atmospheric

385   transport (Longo et al., 2016), atmospheric processing renders Al even more soluble relative to Fe.

386   However, although the soluble ratio of Fe/Al was the same for samples G9-GA01 and M3-GA03, the

387   fractional solubility for Fe differed from 20 % for G9-GA01 to 0.8 % for M3-GA03. We suggest that

388   North African mineral dust was contributing to the composition of M3-GA03, resulting in the low

389   solubility of Fe compared to G9-GA01. This suggestion is supported by isotopic evidence (Conway et

390   al., submitted).

391   For the anthropogenically-derived TEs, Ni, Cu, Zn, Cd and Pb (Figs. 3e-i) and for at least some of

392   samples of the mixed-source TEs (i.e. having crustal and pollution sources; e.g. Mn and Co in Figs. 3b

393   and d), there is some degree of source-dependence in the elemental ratios, with some significant

394   increases from the UCC mass ratios in the total (Shelley et al., 2015) and UHP water soluble fractions

395   (Fig. 3). The higher ratios of the UHP water soluble fraction compared to the total indicates that these

396   TEs are more labile than Al. In addition, studies that have investigated the size distribution of aerosols

397   have found that anthropogenically-derived TEs tend to be associated with fine mode aerosols (< 1 µm

398   diameter), which are more soluble than coarse mode aerosols due to the larger surface area to volume

399   ratio (Duce et al., 1991; Baker and Jickells 2006; Baker and Jickells, 2017). Size fractionated samples

400   were collected during the GA03 cruise, and the smaller size fractions were indeed more soluble than

401   the larger ones for Al, Fe and Co (Landing and Shelley, 2013). Enrichment of TEs with predominantly

402   anthropogenic sources accords with other studies in the North Atlantic, and is most striking for

403   aerosols that did not originate from the sparsely-populated, arid regions of North Africa (e.g. Buck et

404   al., 2010; Gelado-Cabellero et al., 2012; Patey et al., 2015; Shelley et al., 2015).

405

406   **3.3. Aerosol solubility**

407   **3.3.1. Solubility of aerosol TEs as a function of total concentration: UHP water (instantaneous)**
408   **compared to 25 % acetic acid leaches**

409   The UHP water soluble fraction of aerosol Fe and Al determined for all the North Atlantic GA01 and

410   GA03 samples varied by two orders of magnitude (Fig. 4a: Fe = 0.14 - 21 %, median 2.2 %; Al = 0.34

411   - 28 %, median 2.7%). Although a broader range of Fe and Al solubility was observed in this study,

412   both these results and those reported by Buck et al. (2010) using the same approach (Fe = 2.9 - 47%,

413   median = 14%, and Al = 3.7 - 50%, median = 9.5%) broadly agree that the median UHP water soluble

414   fractions of Fe compared to Al in the North Atlantic are similar. While there was considerable overlap

415   in the ranges of fractional solubility of TEs in aerosols from the different regions (e.g. Fe: European

416   1.9 – 21 %; N. American 0.84 – 8.8 %; Marine 1.7 –18 %; High Latitude dust 1.9 – 20 %), the North

417   African samples, identified by their orange colour, high Fe and Al loadings, and definitive AMBTs)

418   formed a distinct cluster of very poorly soluble Fe, or Al ($< 1\%$; Fig. 4a). However, the solubility of

419   the North African ('Saharan') aerosol Fe was 1 – 2 orders of magnitude lower in this study (0.14 –

420 0.57 %) than during the Buck et al. (2010) study (2.9 – 19 %). This supports the hypothesis that TEs

421 from North African aerosols sampled closer to the source (as in this study) are less soluble due to a

422 lesser degree of atmospheric processing and/or larger particle sizes (Baker and Jickells, 2006; Longo

423 et al., 2016).

424 The inverse relationship between total aerosol loading and fractional solubility has previously been

425 reported for Fe (Sholkovitz et al., 2009; 2012; Jickells et al., 2016) and Al (Jickells et al., 2016).

426 Jickells et al. (2016) compiled solubility data from the North Atlantic and found that the general trend

427 between Fe and Al solubility and atmospheric loading was robust over the range of atmospheric

428 loadings found in the North Atlantic, regardless of the leach protocol employed. In this study, both the

429 UHP soluble, and 25 % acetic acid soluble fractions of Fe and Al (Figs 4a and b) were related to

430 atmospheric loading, i.e. the highest loaded North African samples had the lowest solubility. The

431 possible exception to this trend is the fraction of Al that dissolved from North African aerosols

432 following the 25 % acetic acid leach (Fig. 4b). However, it could simply be that we are observing

433 scatter in our data, which is smoothed out in the larger dataset (n > 2000) examined by Jickells et al.

434 (2016). Although we cannot rule out that this effect is the result of the heating step in the 25 % acetic

435 acid leach attacking the alumino-silicate matrix, the similarity in the trend of the solubility of Ti in

436 UHP water and 25 % acetic acid (sharp decrease in solubility with increased aerosol loading, Figs. 4a

437 and b) suggests that matrix attack is minimal. Further experimentation with and without the heating

438 step would help to clarify this issue.

439 Aluminium, Ti, and Fe show very similar behaviour in Figure 4a (sharply decreasing solubility as

440 loading increases). Cobalt, Ni, Cu, Zn and Pb solubilities decrease less strongly as loading increases,

441 whereas Mn and Cd show no clear trend. For the acetic acid leaches (Fig. 4b), Ti follows the same

442 trend as the UHP water leach (Fig. 4a), while Al and Fe plateau at 8-10 % solubility. The other TEs

443 (Mn, Co, Ni, Cu, Zn, Cd and Pb) all show almost no trend with loading. The absence of an inverse

444 trend between solubility and loading has previously been noted for Mn (Jickells et al., 2016). For Co

445 the inverse relationship between UHP water solubility and loading was not observed when using the

446 25 % acetic acid leach, most likely because Co may be associated with the Mn and Fe oxides that are

447 easily reduced using this leach. For Zn and Cd, although their average fractional solubilities (Zn: $37 \pm$

448 28 % and 55 ± 30 %, Cd: 39 ± 23 % and 58 ± 26 % for ultra-high purity water and 25 % acetic acid

449 leaches, respectively) were similar to Mn (32 ± 13 % and 49 ± 13 % for ultra-high purity water and 25

450 % acetic acid leaches, respectively), the range was greater, with several samples from different regions

451 (although not North Africa) being 100% soluble after the second leach.

3.3.2. Solubility of TEs: UHP water (instantaneous) compared to 25 % acetic acid leaches

All ten TEs from the five different categories were less soluble in UHP water than 25 % acetic acid (Fig. 5). This is not a surprising finding given the lower pH of acetic acid compared with UHP water, acetate being a bidentate ligand, the longer contact time of the aerosols with the leach solution, the addition of the hydroxylamine reducing agent and that the fractional solubility of TEs in 25 % acetic acid was calculated using Equation 2 (which sums the UHP water and 25 % acetic acid leach concentrations). In addition, there is some degree of source-dependent variability in the relative proportions of each TE that is released by the two leaches. In general, as with the leaches with UHP water, the North African aerosols were distinctly less soluble in 25% acetic acid compared with aerosols from the other source regions (Fig. 5). Figure 5 highlights the distinction between the lithogenic elements, Al, Fe and Ti, which have uniformly low solubility in UHP water (mostly < 20 %), and extremely low solubility in North African aerosols (< 1 %), and the anthropogenic, pollution-dominated elements, Ni, Cu, Zn, Cd and Pb which have solubility up to 100 %. Manganese and Co have both lithogenic and anthropogenic sources, so are classified as "mixed-source", and have intermediate solubilities. Like all the TEs reported here, Mn solubility in UHP water was significantly less ($p < 0.01$, two-tailed, homoscedastic t-test) in North African aerosols (median solubility = 19 %) than in the non-North African samples (median = 38%), which seems to contrast somewhat with the findings of Baker et al. (2006b) and Jickells et al. (2016) which found that aerosol source had little impact on Mn solubility. However, in common with these earlier studies (Baker et al., 2006b; Jickells et al., 2016), there was no significant source-dependent difference in Mn solubility in 25 % acetic acid (non-North African samples: 49 ± 15%, North African samples: 49 ± 6.4%).

3.3.3. Soluble TEs: UHP water compared to seawater instantaneous leaches

Seawater leaches were conducted on a subset of samples (GA03-2011), to investigate the suitability of seawater as the leach medium in the instantaneous leach (Fig. 6). During this study, Fe solubility in seawater was lower than in UHP water (Fig. 6c). This phenomenon has previously been observed in atmospheric aerosols from the North Atlantic Ocean (Buck et al., 2010). For Fe, only a few samples of North American and Marine provenance conformed to the relationship described by the equation proposed by Buck et al. (2010), with most of our data plotting above the regression line of the Buck et al. (2010) study (Fig. 6c), indicating that our data was relatively more soluble in UHP water compared to seawater than in this earlier study. One possibility is that the higher aerosol Fe loadings we observed during GA03-2011 (this study, maximum = 5650 ng Fe m^{-3}), compared to the A16N-2003 transect (Buck et al. 2010; maximum =1330 ng Fe m^{-3}), resulted in a particle concentration effect (Baker and Jickells, 2006), whereby the relationship between aerosol Fe loading and fractional solubility breaks down because dust on the filter can be a source of soluble Fe but can also scavenge dissolved Fe from the sea water leach solution as it passes through the filter. Given that the link between Fe solubility in seawater and Fe-binding ligand availability is well established (e.g. Rue and

488 Bruland, 1995; Gledhill and Buck, 2012), an alternative explanation for the difference in Fe solubility
489 is that the organic composition of the seawater used as the leach mediums differed between the two
490 studies.

491 Manganese is the only TE that had a slope close to unity (0.98; Fig. 6b), suggesting that solubility
492 estimates were not impacted by the choice of leach medium used. This is consistent with other studies
493 that have found that Mn solubility is less sensitive to the choice of leach media, or to aerosol
494 provenance than other TEs (Baker et al., 2006b; Jickells et al., 2016). Due to the large variability in
495 the data set, there was no significant difference between Mn solubility in UHP water or seawater (32 ±
496 13 % and 24 ± 17 %, respectively; Fig. S3 and Tables S3 and S4, Supplementary Material). Table S5
497 shows which regions had slopes for UHP water versus seawater fractional solubility that did not differ
498 significantly from 1.0 at the 95 % confidence level (t-statistic).

499 Lead was the only TE with all slopes differing significantly from 1.0, and the only TE where the
500 solubility in seawater was higher than in UHP water for virtually every sample (Fig. 6i). As for Pb,
501 most of the Co data falls below the 1:1 line (Fig. 6d), indicating that Co was also generally more
502 soluble in seawater than UHP water. In contrast, the opposite trend was observed for Fe and Ni (Figs
503 6c and e), perhaps due to differences in the availability of metal binding ligands in the seawater used.
504 A challenge of using seawater as the leach medium is that it is difficult to control for natural
505 variability in the types and concentrations of organic ligands. Consequently, it is not possible to
506 determine conclusively why contrasting trends in the fractional solubility of TEs were observed. For
507 this reason, we advocate for the use of UHP water as a common leach medium to facilitate
508 comparisons of solubility resulting from differences in aerosol composition. An additional benefit is
509 the ease of analysis of UHP water compared to seawater.

510

511 **3.4. Visualising marine aerosol sources using multivariate statistical approaches**

512 As the PMF analysis was only able to identify two significant factors accounting for the total aerosol
513 TE concentrations, another multivariate approach was taken. Heirarchical cluster analysis (Ward's
514 method, Euclidian distance) was performed using the R statistical package (v. 3.3.0; R Core Team,
515 2016) to look for trends in the data that might reveal the various aerosol sources. Heirarchical cluster
516 analysis was performed on (1) log transformed total aerosol TE plus NO_3^- concentration data (Fig. 7a),
517 and (2) log transformed TE fractional solubility plus NO_3^- concentration data (Fig. 7b). The NO_3^-
518 concentrations appear in both runs as we wanted to include TEs plus an indicator of anthropogenic
519 pollution.

520   Figure 7a shows two main branches to the dendrogram of the total TE concentration data. One branch

521   groups all the North African and European samples and two North American samples (N2 and N4)

522   together, and the other branch groups all other samples together. Samples closest to each other are the

523   most similar to each other, and those joined in the same groups share similar characteristics.

524   Therefore, in this analysis, the North African samples are grouped together, as are the High Latitude

525   samples. All but three North African samples form a distinct sub-group. The three remaining North

526   African samples (A8, A9 and A11) share more characteristics with the European samples, lending

527   support for mixing of aerosols from the two regions. Counterintuitively, the two European samples

528   with the lowest Fe/Al ratios (E3 and E4) are the ones that are most similar to the two North American

529   samples, which have relatively high Fe/Al ratios of 0.90 and 0.87. The GA01 samples (with the

530   exception of one sample, G15) form a distinct cluster, but with three sub-groups: one is the

531   Greenland/Labrador Sea samples (without G15), and the other two are related to each other but

532   distinct from the Greenland/Labrador Sea samples and are a mixture geographically of the other

533   samples. However, there is a trend, the 'middle' group is the group of samples collected closest to land,

534   the group to the right is the group of samples collected furthest from land. The other groupings are

535   made up of a mixture of North American and Marine samples. This suggests that the Marine samples

536   are comprised predominantly of North American aerosols from more than one source. The only

537   anomaly is the two North American samples that 'look European'.

538   Although there are differences between Figures 7a (total TEs) and 7b (25 % acetic acid fractional

539   solubility; Eq. 2), the general trend of an inverse relationship between TE atmospheric loading and

540   fractional solubility holds, as the North African samples with the highest concentrations and lowest

541   fractional solubilities appear on the left in Figure 7a, and on the right in Figure 7b. In terms of

542   fractional solubility, the N. African samples form a distinct cluster, but this cluster is made up of two

543   sub-groups: one collected during GA03-2010 and one during GA03-2011. The samples collected from

544   near Greenland and the Labrador Sea are also distinct from the other GA01 samples (again with the

545   exception of G15), and also distinct from all other samples. The European samples, all other GA01

546   samples, and three North American samples form a loose cluster. The remaining North American

547   samples and all the Marine samples form another loose cluster.

548   Plotting the data this way still does not allow us to identify the aerosol sources definitively, but it does

549   allow us to visualise which samples have the most similar physico-chemical characteristics and

550   confirms the general trend of a relationship between aerosol loading and fractional solubility and, by

551   extension, bioavailability, even though we have demonstrated that this relationship is not present for

552   all TEs. This knowledge is then useful as a general rule of thumb in biogeochemical models, although

553   clearly other factors also exert controls on aerosol TE solubility. For example, during their

554   investigations of the GA03 aerosols, Wozniak et al., (2013; 2014; 2015) proposed a role for water

555 soluble organic carbon (WSOC) in controlling the solubility of Fe. Desboeufs et al. (2005) also found

556 evidence for a link between total carbon and TE solubility in regions impacted by anthropogenic

557 activity. Thus, the carbon content of aerosols is also implicated as a control on aerosol Fe solubility,

558 but the relationship is frequently not linear.

559

560 **3.5. Choice of leach and modelling TE solubility**

561 The ability of models to replicate subtleties in aerosol TE solubility may prove critical in forecasting

562 ecosystem impacts and responses. Due to the magnitude of North African dust inputs to the North

563 Atlantic region (very high dust inputs result in a high soluble TE aerosol flux despite relatively low

564 fractional solubility), this is a particular challenge and is compounded by additional unknowns such as

565 how aerosol acidity will be impacted by the combined effects of increasing

566 industrialisation/urbanisation, and changes in the magnitude of future mineral dust supply and biomass

567 burning (Knippertz et al., 2015; Weber et al., 2016). In other words, it is important to accurately

568 constrain aerosol TE solubility with high quality data in order to improve the predictive capacity of

569 models. Clearly the choice of leach media and protocol impacts the measured fractional solubility.

570 This is shown in both Figures 4 and 5 and has a number of implications with regard to modelling the

571 impact of atmospheric deposition on marine biogeochemistry. For example, for elements with

572 generally low solubility, such as Fe, the difference between 1 % and 2 % solubility is an increase of

573 100 %, meaning that only half the amount of dust is needed to yield the same amount of dissolved Fe.

574 To complicate matters further, recent research has demonstrated that some diazotrophs are able to

575 directly access particulate Fe (Rubin et al., 2011). The significance of this is that *Trichodesmium* are

576 common in the North Atlantic gyre under the influence of the Saharan plume, and the North African

577 dust samples have higher fractional solubility for Fe using the acetic acid leach. If *Trichosdesmium* are

578 able to access the acetic acid soluble fraction of the aerosol Fe, as the study indicates (Rubin et al.,

579 2011), our data suggests that twentyfold more aerosol Fe is available for uptake than is suggested from

580 the instantaneous UHP water leach. This suggests that in regions where *Trichodesmium* proliferate, we

581 are likely to underestimate bioavailable Fe using the instantaneous UHP water leaching method.

582 There are implications for modelling the impact of atmospheric deposition for other TEs. Although,

583 the lack of source dependent differences in Mn solubility in these aerosols makes modelling Mn

584 solubility simpler, there was still a difference in the fractional solubility calculated from the two

585 leaches (UHP water: 32 ± 13 % and 25 % acetic acid: 49 ± 13 %). However, for Al, there was a large

586 range in solubility:0.3 – 28 % using UHP water and 4.1 – 100 % using 25 % acetic acid. Both ranges

587 far exceed the relatively narrow range used in the MADCOW model (1.5 – 5 %), which has been used

588 to estimate atmospheric inputs based on dissolved Al concentrations in the mixed layer (Measures and

589   Brown, 1996). It is noted, however, that the median values from this study fall within the range used

590   by the MADCOW model (2.7 % and 3.3 % for UHP water and 25 % acetic acid, respectively). We

591   highlight this issue to draw attention to some of the problems inherent in modelling TE solubility and

592   its impact on the chemistry and biogeochemistry of the upper ocean.

593   Given that the different leaching approaches access different fractions of aerosol TEs that can dissolve

594   from aerosols at different rates (e.g. TEs loosely bound to surfaces and TEs that are associated with

595   less reactive phases) (e.g. Kocak et al., 2007; Mackey et al., 2015), we need to conduct experiments

596   that elucidate the relationship between the soluble and bioavailable fractions. In the meantime, we

597   suggest that the 25 % acetic acid leach might be better to estimate the bioavailable fraction given that

598   Fe (and perhaps other TEs) associated with lithogenic particles are directly available to micro-

599   organisms in productive regions and regions with high dust inputs (Rubin et al., 2011) and that aerosol

600   particles can be processed by zooplankton (Schmidt et al., 2016).

601

4. Conclusions

603   Aerosol TE solubility is usually determined using operationally-defined methods, while

604   biogeochemical models require robust relationships between two or more parameters that can be used

605   to predict TE solubility in order to constrain the bioavailable fraction of aerosol TEs. In this study, we

606   used a two-stage leach (UHP water followed by 25 % acetic acid with hydroxylamine hydrochloride)

607   to investigate the fractional solubility of a suite of trace elements (Al, Ti, Mn, Fe, Co, Ni, Cu, Zn, Cd,

608   Pb) from aerosols collected in the North Atlantic during three GEOTRACES research cruises (GA03-

609   2010, GA03-2011 and GA01). Five regions were identified based on air mass back trajectory (AMBT)

610   simulations; i) North Africa, ii) Europe, iii) North America, iv) High Latitude, and v) Marine.

611   However, the AMBTs were not able to sufficiently discriminate aerosol sources within these regions.

612   Of these five categories, the North African aerosols were the most homogeneous in terms of their

613   fractional solubility and elemental ratios. In contrast, samples from the most remote locations, the

614   Marine and High Latitude aerosols, had the most spread in their fractional solubility and elemental

615   ratios. Elemental ratios were discussed rather than enrichment factors normalised to UCC composition

616   since earlier work highlighted that the UCC ratios are not representative of the North African mineral

617   dust end-member, which dominates aerosol supply in much of the study area.

618   We observed an inverse relationship between the fractional solubility of Al, Ti, Fe, Ni, Cu and Pb and

619   aerosol loading for all leach media (UHP water, filtered seawater, and 25 % acetic acid with

620   hydroxylamine hydrochloride). However, Mn, Zn and Cd fractional solubility appears to be

621   independent of atmospheric loading. For Co, the inverse relationship between UHP water solubility

622   and loading was not observed when using the 25 % acetic acid leach, most likely because Co may be

623   associated with the Mn and Fe oxides that are easily reduced using the 25 % acetic acid leach. Further

624   work is required to assess exactly which fraction is accessed by the various leach protocols in order to

625   understand links between the soluble and bioavailable fractions.

626

Data availability

628   Data is available at BCO-DMO (GA03; www.bco-dmo.org) and LEFE-CYBER (GA01;

629   (www.obsvlfr.fr/proof/php/GEOVIDE/GEOVIDE.php), and on request from the lead author.

Acknowledgements

631   Many thanks to the captains and crews of the RV Knorr (GA03-2010 and 2011) and NO Pourquoi

632   Pas? (GA01), the chief scientists (GA03 = Bob Anderson, Ed Boyle, Greg Cutter; GA01 = Geraldine

633   Sarthou and Pascale Lherminier), Alex Baker for the loan of the aerosol sampler used on GA01, and

634   Alina Ebling Petroc Shelley, Alex Landing and Sarah Huff for their help with sample processing and

635   analysis. This work was supported by grants to WML (NSF-OCE 0752832, 0929919 and 1132766),

636   and GS (ANR-13-B506-0014 and ANR-12-PDOC-0025-01). RUS was supported by a LabexMER

637   International Postdoctoral Fellowship and CG29 Postdoctoral Fellowship. A portion of this work was

638   performed at the National High Magnetic Field Laboratory, which is supported by National Science

639   Foundation Cooperative Agreement No. DMR-1157490 and the State of Florida. The aerosol

640   digestions for GA01 were undertaken in the geochemistry clean room at Ifremer (Centre de Bretagne).

641   Trace element determination for GA01 was conducted at the Pôle de Spectrométrie Océan at the

642   Institut Universitaire Européen de la Mer with the support and guidance of Claire Bollinger and

643   Marie-Laure Rouget. Finally, we thank Karine Desbeoufs and an anonomous reviewer for their

644   critiques that have contributed to the improvement of this manuscript.

645

References

647   Achterberg, E. P., Moore, C.M., Henson, S. A., Steigenberger, S., Stohl, A., Eckhardt, S., Avendano,

648   LC., Cassidy, M., Hembury, D., Klar, J.K., Lucas, M.I., Macey, A.I., Marsay, C.M., and, Ryan-

649   Keogh, T.J.: Natural iron fertilization by the Eyjafjallajökull volcanic eruption, Geophys. Res. Lett.,

650   40, 921-926, http://doi.org/10.1002/grl.50221, 2013.

651   Adams, A. M., Prospero, J.M., and Zhang, C.: CALIPSO-Derived Three-Dimensional Structure of

652   Aerosol over the Atlantic Basin and Adjacent Continents, Journal of Climate, 25, 6862-6879,

653   http://doi.org/10.1175/JCLI-D-11-00672.1, 2012.

654   Aguilar-Islas, A. M., Wu, J., Rember, R., Johansen, A.M. and Shank, L. M.: Dissolution of aerosol-

655   derived iron in seawater: Leach solution chemistry, aerosol type, and colloidal iron fraction, Marine

656   Chemistry, 120, 25-33., 2010.

657   Arnalds, O.: Soils of Iceland, Jökull, 58, 409-421, 2004.

Baker, A. R., Adams, C., Bell, T.G., Jickells, T.D., and Ganzeveld, L.: Estimation of atmospheric nutrient inputs to the Atlantic Ocean from 50N to 50S based on large-scale filed sampling: Iron and other dust-associated elements, Global Biogeochem. Cycles, 27, 755-767, http://doi.org/10.1002gbc.20062, 2013, 2013.

Baker, A. R., and, Croot, P. L.: Atmospheric and marine controls on aerosol iron solubility in seawater., Marine Chemistry., 120, 4-13, 2010.

Baker, A. R., and Jickells, T.D.: Mineral particle size as a control on aerosol iron solubility., Geophys. Res. Lett., 33, http://doi.org/10.1029/2006GL026557, 2006.

Baker, A. R., and, Jickells, T.D.: Atmospheric deposition of soluble trace elements along the Atlantic Meridional Transect (AMT), Progress in Oceanography, 158, 41-51, 10.1016/j.pocean.2016.10.002, 2017.

Baker, A. R., Jickells, T. D., Biswas, K. F., Weston, K., and French, M.: Nutrients in atmospheric aerosol particles along the Atlantic Meridional Transect, Deep Sea Research Part II: Topical Studies in Oceanography, 53, 1706-1719, 2006a.

Baker, A. R., Jickells, T. D., Witt, M., and Linge, K. L.: Trends in the solubility of iron, aluminium, manganese and phosphorus in aerosol collected over the Atlantic Ocean, Marine Chemistry, 98, 43-58, 2006b.

Baker, A. R., Landing, W.M., Bucciarelli, E., Cheize, M., Fietz, S., Hayes, C.T., Kadko, D., Morton, P.L., Rogan, N., Sarthou, G., Shelley, R.U., Shi, Z., Shiller, A., and, van Hulten, M.M.P.: Trace element and isotope deposition across the air–sea interface: progress and research needs, Philosophical Transactions of the Royal Society A: Mathematical, Physical and Engineering Sciences, 374, http://doi.org/10.1098/rsta.2016.0190, 2016.

Baratoux, D., Mangold, N., Arnalds, O., Bardintzeff, J.-M., Platevoët, B., Grégoire, M., and Pinet, P.: Volcanic sands of Iceland - Diverse origins of aeolian sand deposits revealed at Dyngjusandur and Lambahraun, Earth Surf. Process. Landforms, 36, 1789-1808, 10.1002/esp.2201, 2011.

Ben-Ami, Y., Koren, I., Rudich, Y., Artaxo, P., Martin, S.T., and Andreae, M.O.: Transport of North African dust from the Bodele depression to the Amazon Basin: a case study, Atmos. Chem. Phys., 10, 7533-7544, http://doi.org/10.5194/acp-10-7533-2010, 2010.

Berger, J. M., Lippiatt, S.M., Lawrence, M.G., and Bruland, K.W.: Application of a chemical leach technique for estimating labile particulate aluminum, iron, and manganese in the Columbia River plume and coastal waters off Oregon and Washington., Journal of Geophysical Research, 113, http://doi.org/10.1029/2007JC004703, 2008.

Bridgestock, L., Rehkämper,M., van de Flierdt,T., Murphy, K., Khondoker, R., Baker, A. R., Chance, R., Strekopytov, S., Humphreys-Williams, E., and Achterberg E.P.: The Cd isotope composition of atmospheric aerosols from the Tropical Atlantic Ocean, Geophys. Res. Lett., 44, 2932-2940, http://doi.org/10.1002/2017GL072748, 2017.

Buck, C. S., Landing, W.M., and Resing, J.: Pacific Ocean aerosols: Deposition and solubility of iron, aluminum, and other trace elements, Marine Chemistry, 157, 117-130, http://dx.doi.org/10.1016/j.marchem.2013.09.005, 2013.

697 Buck, C. S., Landing, W.M., Resing, J. A., Lebon, G. T.: Aerosol iron and aluminum solubility in the
698 northwest Pacific Ocean: Results from the 2002 IOC cruise, Geochemistry, Geophysics, Geosystems.,
699 7, http://doi.org/10.1029/2005GC000977, 2006.

700 Buck, C. S., Landing, W.M., Resing, J.A. and Measures, C.I.: The solubility and deposition of aerosol
701 Fe and other trace elements in the North Atlantic Ocean: Observations from the A16N CLIVAR/CO$_2$
702 repeat hydrography section., Marine Chemistry., 120, 57-70, 2010.

703 Bullard, J. E., Baddock, M., Bradwell, T., Crusius, J., Darlington, E., Gaiero, D., Gassó, S.,
704 Gisladottir, G., Hodgkins, R., McCulloch, R., McKenna-Neuman, C., Mockford, T., Stewart, H., and,
705 Thorsteinsson, T.: High-latitude dust in the Earth system, Reviews of Geophysics, 54, 447-485,
706 http://doi.org/10.1002/2016RG000518, 2016.

707 Cheize, M., Sarthou, G., Croot, P., Bucciarelli, E., Baudoux, A.-C., and Baker, A.: Iron organic
708 speciation determination in rainwater using cathodic stripping voltammetry, Analytica Chimica Acta,
709 726, 45-54, 2012.

710 Chiapello, I., Bergametti, G., Chatenet, B., Bousquet, P., Dulac, F., and Soares, E. S.: Origins of
711 African dust transported over the northeastern tropical Atlantic, Journal of Geophysical Research:
712 Atmospheres, 102, 13701-13709, 10.1029/97jd00259, 1997.

713 Chueinta, W., Hopke, P. K., and Paatero, P.: Investigation of sources of atmospheric aerosol at urban
714 and suburban residential areas in Thailand by positive matrix factorization, Atmospheric Environment,
715 34, 3319-3329, http://dx.doi.org/10.1016/S1352-2310(99)00433-1, 2000.

716 Conway, T. M., and John, S.G.: Quantification of dissolved iron sources to the North Atlantic Ocean,
717 Nature, 511, 212-215, http://doi.org/10.1038/nature13482. 2014.

718 Conway, T.M., Shelley, R.U., Aguilar-Islas, A.M., Landing, W.M., Mahowald, N.M., and John, S.G.:
719 Iron isotopes reveal and important anthropogenic aerosol iron flux to the North Atlantic. Submitted to:
720 Nature Communications.

721 de Leeuw, G., Guieu, C., Arneth, A., Bellouin, N., Bopp, L., Boyd, P.W., Denier van der Gon, H.A.C.,
722 Desboeufs, K.V., Dulac, F., Facchini, M.C., Gantt, B., Langmann, B., Mahowald, N.M., Maranon, E.,
723 O'Dowd, C., Olgun, N., Pulido-Villena, E., Rinaldi, M., Stephanou, E.G., and Wagener, T. : Ocean-
724 atmosphere interactions of particles, in: Ocean-atmosphere interactions of gases and particles, edited
725 by: Liss, P. S., and Johnson, M.T., Springer-Verlag, Berlin, 171-245, 2014.

726 Desboeufs, K. V., Sofikitis, A., Losno, R., Colin, J. L. and Ausset, P.: Dissolution and solubility of
727 trace metals from natural and anthropogenic aerosol particulate matter., Chemosphere, 58, 195-203.,
728 2005.

729 Doherty, O. M., Riemer, N., and Hameed, S.: Role of the convergence zone over West Africa in
730 controlling Saharan mineral dust load and transport in the boreal summer, Tellus B, 66,
731 http://doi.org/10.3402/tellusb.v66.23191, 2014.

732 Fishwick, M. P., Sedwick, P.N., Lohan, M.C., Worsfold, P.J., Buck, K.N., Church, T.M., and Ussher,
733 S.J.: The impact of changing surface ocean conditions on the dissolution of aerosol iron, Global
734 Biogeochem. Cycles, 28, 1235-1250, http://doi.org/10.1002/2014GB 004921, 2014.

735 Gelado-Caballero, M. D., López-García, P., Prieto, S., Patey, M.D., Collado, C., Hérnández-Brito, J.J.:
736 Long-term aerosol measurements in Gran Canaria, Canary Islands: Particle concentration, sources and
737 elemental composition, Journal of Geophysical Research: Atmospheres, 117, D03304,
738 http://doi.org/10.1029/2011jd016646, 2012.

739 GEOTRACES Planning Group, GEOTRACES Science Plan. Baltimore, Maryland:
740 Scientific Committee on Oceanic Research, http://www.geotraces.org/science/science-plan, 2006.

741 Gledhill, M., and Buck, K. N.: The organic complexation of iron in the marine environment: a review,
742 Frontiers in Microbiology, https://doi.org/10.3389/fmicb.2012.00069, 2012.

743 Hatta, M., Measures, C. I., Wu, J., Roshan, S., Fitzsimmons, J. N., Sedwick, P., and, and Morton, P.:
744 An overview of dissolved Fe and Mn Distributions during the 2010–2011 U.S. GEOTRACES north
745 Atlantic Cruises: GEOTRACES GA03, Deep Sea Research Part II: Topical Studies in Oceanography,
746 http://dx.doi.org/10.1016/j.dsr2.2014.07.005, 2015.

747 Helmers, E., and Schrems, O.: Wet deposition of metals to the tropical North and the South Atlantic
748 Ocean, Atmospheric Environment, 29, 2475-2484, 1995.

749 Jickells, T. D., Baker, A. R., and Chance, R.: Atmospheric transport of trace elements and nutrients to
750 the oceans, Philosophical Transactions of the Royal Society A: Mathematical, Physical and
751 Engineering Sciences, 374, http://doi.org/10.1098/rsta.2015.0286, 2016.

752 Jickells, T. D., An, Z.S., Andersen, K.K., Baker, A.R., Bergametti, G., Brooks, N., Cao, J.J., Boyd,
753 P.W., Duce, R.A., Hunter, K.A., Kawahata, H., Kubilay, N., laRoche, J., Liss, P.J., Mahowald, N.,
754 Prospero, J.M., Ridgwell, A.J., Tegen, I., and Torres, R.: Global iron connections between desert dust,
755 ocean biogeochemistry and climate., Science, 308, 67-71, 2005.

756 Johansen, A., Siefert, R.L., Hoffmann, M.R.: Chemical composition of aerosols collected over the
757 tropical North Atlantic Ocean, Journal of Geophysical Research, 105, 15277-15312, 2000.

758 Johnson, B. T., Osborne, S.R., Haywood, J.M., and Harrison, M.A.J.: Aircraft measurements of
759 biomass burning aerosol over West Africa during DABEX, J. Geophys. Res., 113,
760 10.1029/2007JD009451, 2008.

761 Kim, G., Alleman, L.Y., and Church, T.M.: Atmospheric depositional fluxes of trace elements, 210Pb,
762 and 7Be to the Sargasso Sea, Global Biogeochemical Cycles, 13, http://doi.org/1183-1192,
763 10.1029/1999gb900071, 1999.

764 Knippertz, P., Coe, H., Chiu, J. C., Evans, M.J., Fink, A.H., Kalthoff, N., Liousse, C., Mari, C.,
765 Allan, R.P., Brooks, B., Danour, S., Flamant, C., Jegede, O.O., Lohou, F., and, Marsham, J.H.: The
766 DACCIWA Project: Dynamics–Aerosol–Chemistry–Cloud Interactions in West Africa, Bulletin of the
767 American Meteorological Society, 96, 1451-1460, 10.1175/BAMS-D-14-00108.1, 2015.

768 Koçak, M., Kubilay, N., Herut, B., and Nimmo, M.: Trace Metal Solid State Speciation in Aerosols of
769 the Northern Levantine Basin, East Mediterranean, Journal of Atmospheric Chemistry, 56, 239-257,
770 http://doi.org/10.1007/s10874-006-9053-7, 2007.

771 Lafon, S., Sokolik, I. N., Rajot, J. L., Caquineau, S. and Gaudichet, A.: Characterization of iron oxides
772 in mineral dust aerosols: Implications for light absorption, J. Geophys. Res., 111,
773 10.1029/2005JD007016, 2006.

774   Laing, J. R., Hopke, P.K., Hopke, E.F., Husain, L., Dutkiewicz, V.A., Paatero, J., and Viisanen, Y.:
775   Positive Matrix Factorization of 47 Years of Particle Measurements in Finnish Arctic, Aerosol and Air
776   Quality Research, 15, 188-207, http://doi.org/10.4209/aaqr.2014.04.0084, 2015.

777   Landing, W.M., and Shelley, R.U.: Particle size effects on aerosol iron solubility from the U.S.
778   GEOTRACES North Atlantic Zonal Transect (2010, 2011), ASLO 2013 Aquatic Sciences Meeting,
779   2013.

780   Longhurst, A.: Ecological Geography of the Sea., Academic Press., San Diego, 1998.

781   Longo, A. F., Feng, Y., Lai, B., Landing, W.M., Shelley, R.U., Nenes, A., Mihalopoulos, N., Violaki,
782   K., and, Ingall, E.D.: Influence of Atmospheric Processes on the Solubility and Composition of Iron in
783   Saharan Dust, Environmental Science & Technology, 50, 6912-6920,
784   http://doi.org/10.1021/acs.est.6b02605, 2016.

785   Mackey, K. R. M., Chien, C.-T., Post, A.F., Saito, M.A., and Paytan, A.: Rapid and gradual modes of
786   aerosol trace metal dissolution in seawater, Frontiers in Microbiology, 5, 1-11,
787   http://doi.org/10.3389/fmicb.2014.00794, 2015.

788   Maring, H., Settle, D.M., Buat-Ménard, P., Dulac, F., and, Patterson, C.C.: Stable lead isotopes tracers
789   of air mass trajectories in the Mediterranean region, Nature, 300, 154-156, 1987.

790   Marticorena, B., Chatenet, B., Rajot, J. L., Traoré, S., Coulibaly, M., Diallo, A., Koné, I., Maman, A.,
791   Ndiaye, T., and Zakou, A.: Temporal variability of mineral dust concentrations over West Africa:
792   analyses of a pluriannual monitoring from the AMMA Sahelian Dust Transect, Atmos. Chem. Phys.,
793   10, 8899-8915, 10.5194/acp-10-8899-2010, 2010.

794   McConnell, C. L., Highwood, E.J., Coe, H., Formenti, P., Anderson, B., Osborne, S., Nava, S.,
795   Desboeufs, K., Chen, G., and Harrison, M.A.J.: Seasonal variations of the physical and optical
796   characteristics of Saharan dust: Results from the Dust Outflow and Deposition to the Ocean (DODO)
797   experiment, Journal of Geophysical Research: Atmospheres, 113, D14S05, 10.1029/2007jd009606,
798   2008.

799   Measures, C.I., and Brown E.T.: Estimating dust input to the Atlantic Ocean using surface water Al
800   concentrations, in, The Impact of desert dust across the Mediterranean, edited by S. Guerzoni and R.
801   Chester, pp.301-311, Kluwer: Dordrecht, 1996.

802   Menzel-Barraqueta, J.-L., Schlosser, C., Planquette, H., Gourain, A., Cheize, M., Boutorh, J., Shelley,
803   R., Pereira Contreira, L., Gledhill, M., Hopwood, M.J., Lherminier, P., Sarthou, G. and Achterberg,
804   E.P. Aluminium in the North Atlantic Ocean and the Labrador Sea (GEOTRACES GA01 section):
805   roles of continental inputs and biogenic particle removal. Biogeosciences Discuss.,
806   https://doi.org/10.5194/bg-2018-39, this issue.

807   Morton, P. L., Landing, W.M.,Hsu, S.-C., Milne, A., Aguilar-Islas, A.M., Baker, A.R., Bowie, A.R.,
808   Buck, C.S., Gao, Y., Gichuki, S., Hastings, M.G., Hatta, M., Johansen, A. M., Losno, R., Mead, C.,
809   Patey, M.D., Swarr, G., Vandermark, A., Zamora, L.M.: Methods for the sampling and analysis of
810   marine aerosols: results from the 2008 GEOTRACES aerosol intercalibration experiment, Limnology
811   and Oceanography: Methods, 11, 62-78, 2013.

812   Oladottir, B. A., Sigmarsson, O., Larsen, G., and Devidal, J.L.: Provenance of basaltic tephra from
813   Vatnajokull subglacial volcanos, iceland, as determined by major- and trace-element analyses, The
814   Holocene, 21, 1037-1048, 10.1177/0959683611400456, 2011.

815   Patey, M. D., Achterberg, E.P., Rijkenberg, M.J., and Pearce, R.: Aerosol time-series measurements
816   over the tropical Northeast Atlantic Ocean: Dust sources, elemental, composition and mineralogy,
817   Marine Chemistry, 174, 103-119, http://dx.doi.org/10.1016/j.marchem.2015.06.004, 2015.

818   Petzold, A., Rasp, K., Weinzierl, B., Esselborn, M., Hamburger, T., Dörnbrack, A., Kandler, K.,
819   Schütz, L., Knippertz, P., Fiebig, M., and Virkkula, A.: Saharan dust absorption and refractive index
820   from aircraft-based observations during SAMUM 2006, Tellus B, 61, 118-130, 10.1111/j.1600-
821   0889.2008.00383.x, 2009.

822   Planquette, H., Gourain, A., Cheize, M., Menzel Barraqueta, J.L., Boutorh, J., Shelley, R., Pereira
823   Contreira, L., Lacan, F., Lherminier, P. and Sarthou, G. Particulate trace elements in the North
824   Atlantic along the GEOVIDE section (GEOTRACES GA01), ASLO 2016 Ocean Sciences Meeting,
825   2016.

826   Powell, C. F., Baker, A.R., Jickells, T.D., Bange, H.W., Chance, R.J., Yodle, C.: Estimation of the
827   atmospheric flux of nutrients and trace metals to the eastern tropical North Atlantic Ocean, Journal of
828   the Atmospheric Sciences, 4029-4045, http://doi.org/10.1175/JAS-D-15-0011.1, 2015.

829   Prospero, J. M., Bullard, J.E., and Hodgkins, R.: High-Latitude Dust Over the North Atlantic: Inputs
830   from Icelandic Proglacial Dust Storms, Science, 335, 1078-1082,
831   http://doi.org/10.1126/science.1217447, 2012.

832   Prospero, J. M., Ginoux, P., Torres, O., Nicholson, S.E. and Thomas, T.E.: Environmental
833   characterization of global sources of atmospheric dust identified with the Nimbus 7 Total Ozone
834   Mapping Spectrometer (TOMS) absorbing aerosol product., Reviews of Geophysics., 40,
835   10.1029/2000RG000095, 2002.

836   Prospero, J. M., Glaccum, R.A. and Nees, R.T.: Atmospheric transport of soil dust from Africa to
837   South America., Nature., 289, 570-572., 570-572., 1981.

838   R Core Team: R: A Language and Environmental for Statistical Computing. https://www.R-
839   project.org., 2016.

840   Rolph, G.D., Real-time Environmental Applications and Display sYstem (READY) Website
841   (http://ready.arl.noaa.gov). NOAA Air Resources Laboratory, Silver Spring, MD, 2017.Rubin, M.,
842   Berman-Frank, I., and Shaked, Y.: Dust- and mineral-iron utilization by the marine dinitrogen-fixer
843   Trichodesmium, Nature Geosci, 4, 529-534, 2011.

844   Rudnick, R. L., and Gao, S.: Composition of the continental crust, in: Treatise on Geochemistry,
845   edited by: Holland, H. D., and Turekian, K.K., Elsevier, Oxford, 1-64, http://dx.doi.org/10.1016/B0-
846   08-043751-6/03016-42003.

847   Rue, E. L., and Bruland, K. W. : Complexation of iron (III) by natural organic ligands in the Central
848   North Pacific as determined by a new competiative ligand equilibrium/ adsorptive cathodic stripping
849   voltammetric method, Marine Chemistry, 50, 117-138, 1995.

850   Sarthou, G., Baker, A.R., Blain, S., Achterberg, E.P., Boye, M., Bowie, A.R., Croot, P., Laan, P., de
851   Baar, H.J. W., Jickells, T.D. and Worsfold, P.J.: Atmospheric iron deposition and sea-surface
852   dissolved iron concentrations in the eastern Atlantic Ocean., Deep Sea Research Part I: Oceanographic
853   Research Papers., 50, 1339-1352., 2003.

854   Scheuvens, D., Schütz, L., Kandler, K., Ebert, M., and Weinbruch, S.: Bulk composition of northern
855   African dust and its source sediments — A compilation, Earth-Science Reviews, 116, 170-194,
856   http://dx.doi.org/10.1016/j.earscirev.2012.08.005, 2013.

857 Schmidt, K., Schlosser, C., Atkinson, A., Fielding, S., Venables, H.J., Waluda, C.M., and Achterberg,
858 E.P.: Zooplankton gut passage mobilizes lithogenic iron for ocean productivity, Current Biology, 26,
859 2667-2673, https://doi.org/10.1016/j.cub.2016.07.058, 2016.

860 Sedwick, P. N., Sholkovitz, E.R. and Church, T.M.: Impact of anthropogenic combustion emissions on
861 the fractional solubility of aerosol iron: evidence from the Sargasso Sea., Geochemistry, Geophysics,
862 Geosystems., 8, http://doi.org/10.1029/2007GC001586, 2007.

863 Sippula, O., Stengel, B., Sklorz, M., Streibel, T., Rabe, R., Orasche, J., Lintelmann, J., Michalke, B.,
864 Abbaszade, G., Radischat, C., Gröger, T., Schnelle-Kreis, J., Harndorf, H., and Zimmermann, R.:
865 Particle Emissions from a Marine Engine: Chemical Composition and Aromatic Emission Profiles
866 under Various Operating Conditions, Environmental Science & Technology, 48, 11721-11729,
867 10.1021/es502484z, 2014.

868 Shaked, Y., and Lis, H.: Dissassembling iron availability to phytoplankton, Frontiers in Microbiology,
869 3, http://doi.org/10.3389/fmicb.2012.00123, 2012.

870 Shelley, R. U., Morton, P.L. and Landing, W.M.: Elemental ratios and enrichment factors in aerosols
871 from the US-GEOTRACES North Atlantic transects, Deep Sea Research Part II: Topical Studies in
872 Oceanography, 116, 262-272, http://dx.doi.org/10.1016/j.dsr2.2014.12.005, 2015.

873 Shelley, R. U., Roca-Martí, M., Castrillejo, M., Sanial, V., Masqué, P., Landing, W.M., van Beek, P.,
874 Planquette, H., and, Sarthou, G.: Quantification of trace element atmospheric deposition fluxes to the
875 Atlantic Ocean (> 40°N; GEOVIDE, GEOTRACES GA01) during spring 2014, Deep Sea Research
876 Part I: Oceanographic Research Papers, 119, 34-49, http://doi.org/10.1016/j.dsr.2016.11.010, 2017.

877 Sholkovitz, E., R., Sedwick, P.N. and Church, T.M.: Influence of anthropogenic combustion emissions
878 on the deposition of soluble aerosol iron to the ocean: Empirical estimates for island sites in the North
879 Atlantic., Geochimica et Cosmochimica Acta., 73, 3981-4003., 2009.

880 Sholkovitz, E., R., Sedwick, P.N., Church, T.M., Baker, A.R., and Powell, C.F.: Fractional solubility
881 of aerosol iron: Synthesis of a global-scale data set, Geochimica et Cosmochimica Acta, 89, 173-189,
882 2012.

883 Skonieczny, C., Bory, A. Bout-Roumazeilles, V., Abouchami, W., Galer, S. J. G., Crosta, X. Stuut,
884 J.-B., I. Meyer, Chiapello, I., Podvin, T., Chatenet, B., Diallo, A., and Ndiaye, T.: The 7–13 March
885 2006 major Saharan outbreak: Multiproxy characterization of mineral dust deposited on the West
886 African margin, Journal of Geophysical Research, 116, http://doi.org/10.1029/2011JD016173, 2011.

887 Stein, A.F., Draxler, R.R, Rolph, G.D., Stunder, B.J.B, Cohen, M.D., and Ngan, F.: NOAA's
888 HYSPLIT atmospheric transport and dispersion modeling system, Bull. Amer. Meteor. Soc., 96, 2059-
889 2077, http://doi.org/10.1175/BAMS-D-14-00110.1, 2015.

890 Tonnard, M., Planquette, H., Bowie, A.R., van der Merwe, P., Gallinari, M., Desprez de Gésincourt,
891 F., Germain, Y., Gourain, A., Benetti, M., Reverdin, G., Treguer, P., Boutorh, J., Cheize, M., Menzel-
892 Barraqueta, J.L., Pereira-Contreira, L., Shelley, R., Lherminier, P., and Sarthou, G. Dissolved iron in
893 the North Atlantic Ocean and Labrador Sea along the GEOVIDE section (GEOTRACES section
894 GA01), Submitted to Biogeosciences Discuss., this issue.

895 Ussher, S. J., Achterberg, E.P., Powell, C., Baker, A.R., Jickells, T.D., Torres, R., and Worsfold, P.J.:
896 Impact of atmospheric deposition on the contrasting iron biogeochemistry of the North and South
897 Atlantic Ocean, Global Biogeochemical Cycles, 27, 1096-1107, http://doi.org/10.1002/gbc.20056,
898 2013.

899   Weber, R. J., Guo, H., Russell, A.G., and Nenes, A.: High aerosol acidity despite declining
900   atmospheric sulfate concentrations over the past 15 years, Nature Geosci, 9, 282-285,
901   http://doi.org/10.1038/ngeo2665

902   Wozniak, A. S., Shelley, R.U., McElhenie, S.D., Landing, W.M., and Hatcher, P.G.: Aerosol water
903   soluble organic matter characteristics over the North Atlantic Ocean: Implications for iron-binding
904   ligands and iron solubility, Marine Chemistry, 173, 162-172,
905   http://dx.doi.org/10.1016/j.marchem.2014.11.002, 2015.

906   Wozniak, A. S., Shelley, R.U., Sleighter, R.L., Abdulla, H.A.N., Morton, P.L., Landing, W.M., and
907   Hatcher, P.G.: Relationships among aerosol water soluble organic matter, iron and aluminum in
908   European, North African, and Marine air masses from the 2010 US GEOTRACES cruise, Marine
909   Chemistry, 154, 24-33, http://dx.doi.org/10.1016/j.marchem.2013.04.011, 2013.

910   Wozniak, A. S., Willoughby, A. S., Gurganus, S. C., and Hatcher, P. G.: Distinguishing molecular
911   characteristics of aerosol water soluble organic matter from the 2011 trans-North Atlantic US
912   GEOTRACES cruise, Atmos. Chem. Phys., 14, 8419-8434, 10.5194/acp-14-8419-2014, 2014.

913   Zurbrick, C., Boyle, E., Kayser, R., Reuer, M., Wu, J., Planquette, H., Shelley, R., Boutorh, J., Cheize,
914   M., Contreira, L., Menzel, J.L. and Sarthou, G. Dissolved Pb and Pb isotopes in the North Atlantic
915   from the GEOVIDE transect (GEOTRACES GA-01) and heir decadal evolution. Biogeosciences
916   Discuss, https://doi.org/10.5194/bg-2018-29.
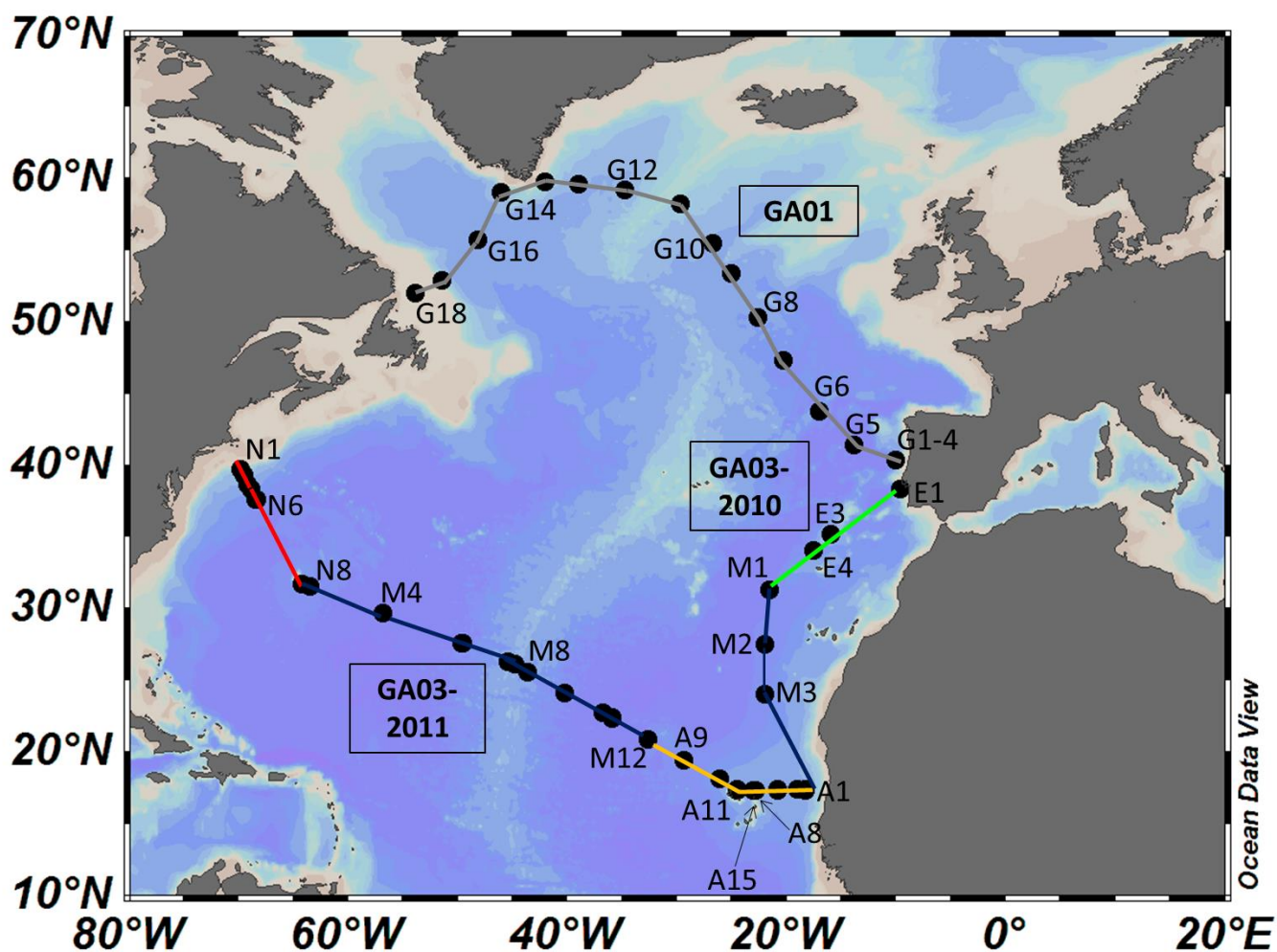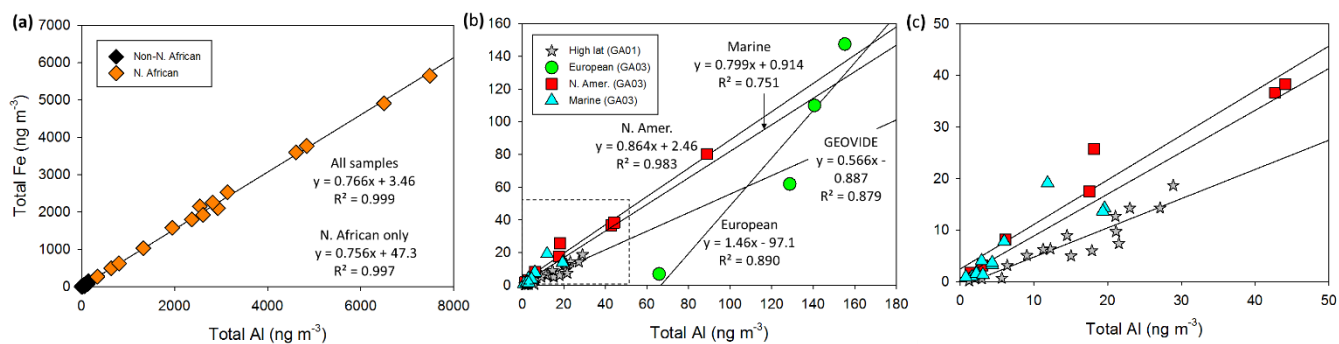
917

918
919

920

921

922

923

Figure 1

924
925
926
927
928
929

930

Figure 2

931
932
933

934
935 **Figure 3**
936
937
938
939
940
941
942
943
944
945
946

947
948   **Figure 4**

949

950

951

952   **Figure 5**

953

954

955

956 **Figure 6**

957
958
959
960
961
962
963

964
965
966
967

968
969 **Figure 7**
970
971
972
973
974
975
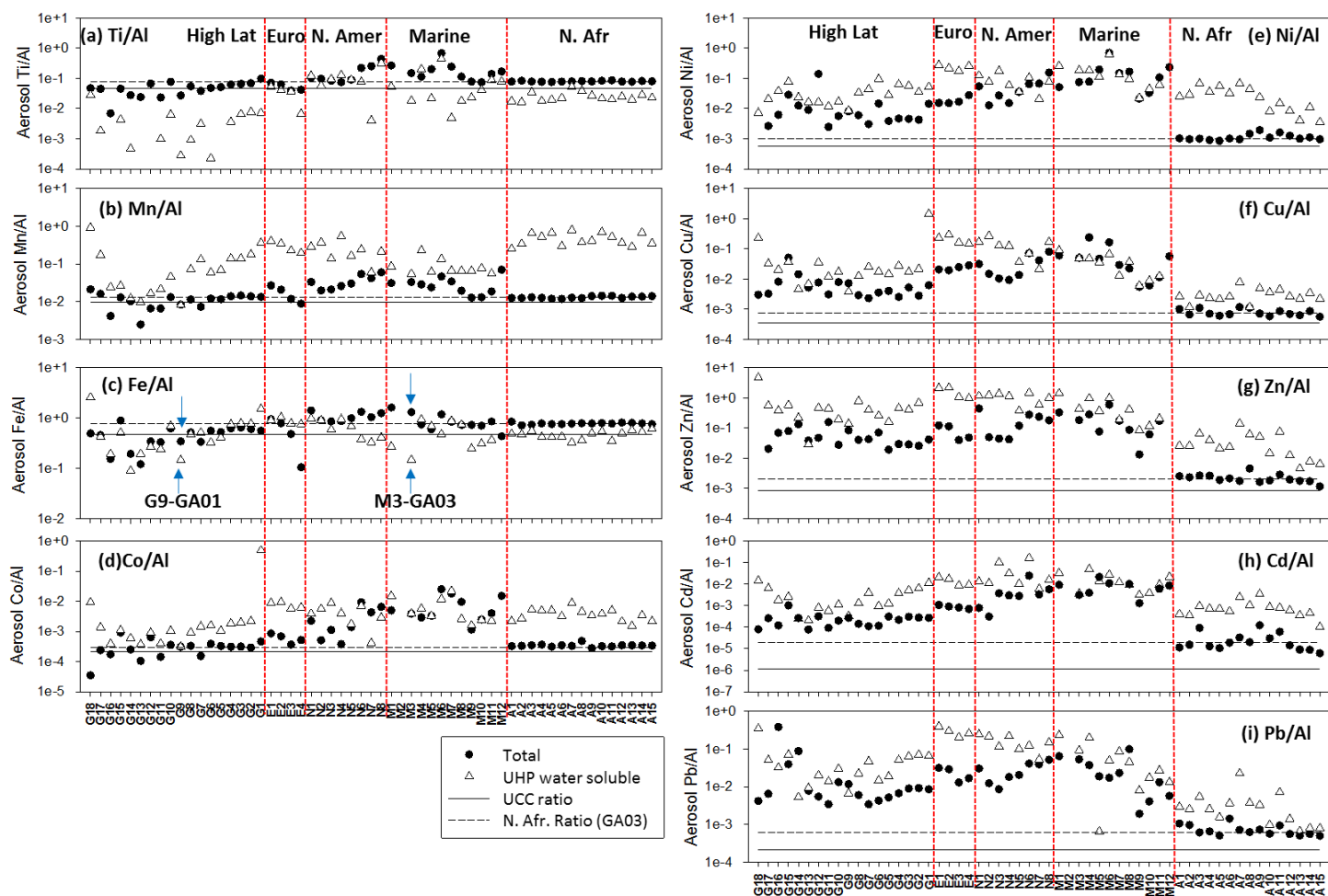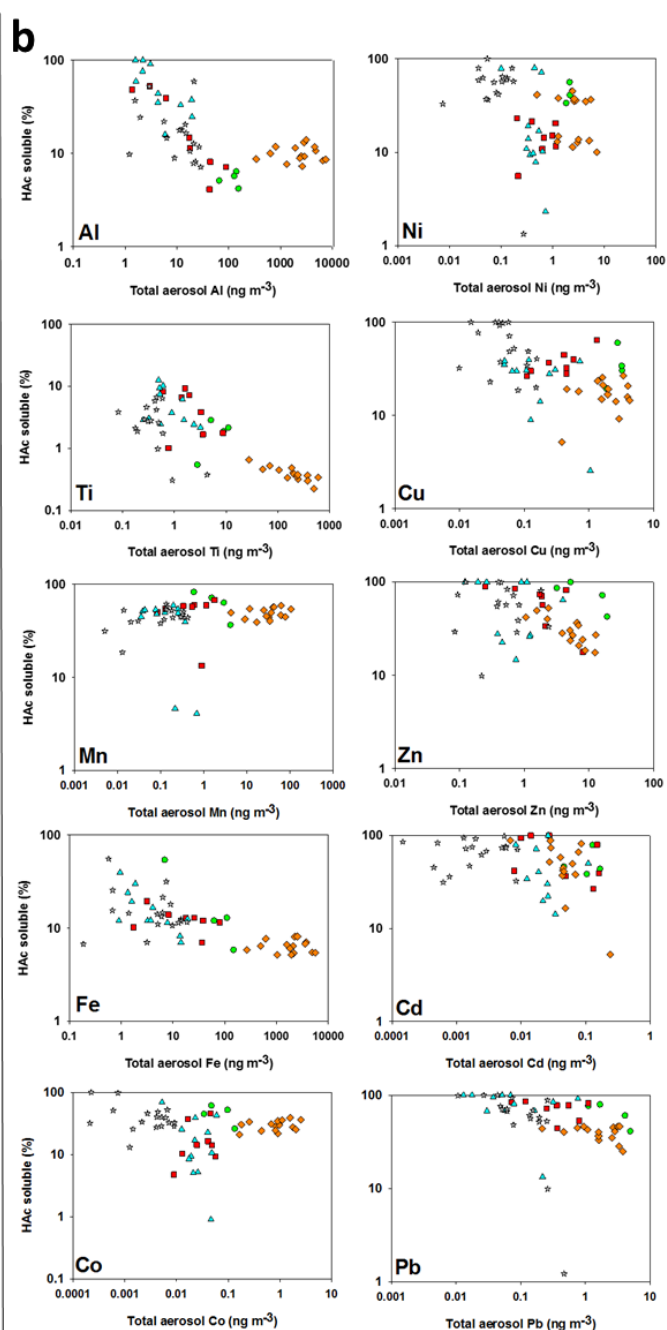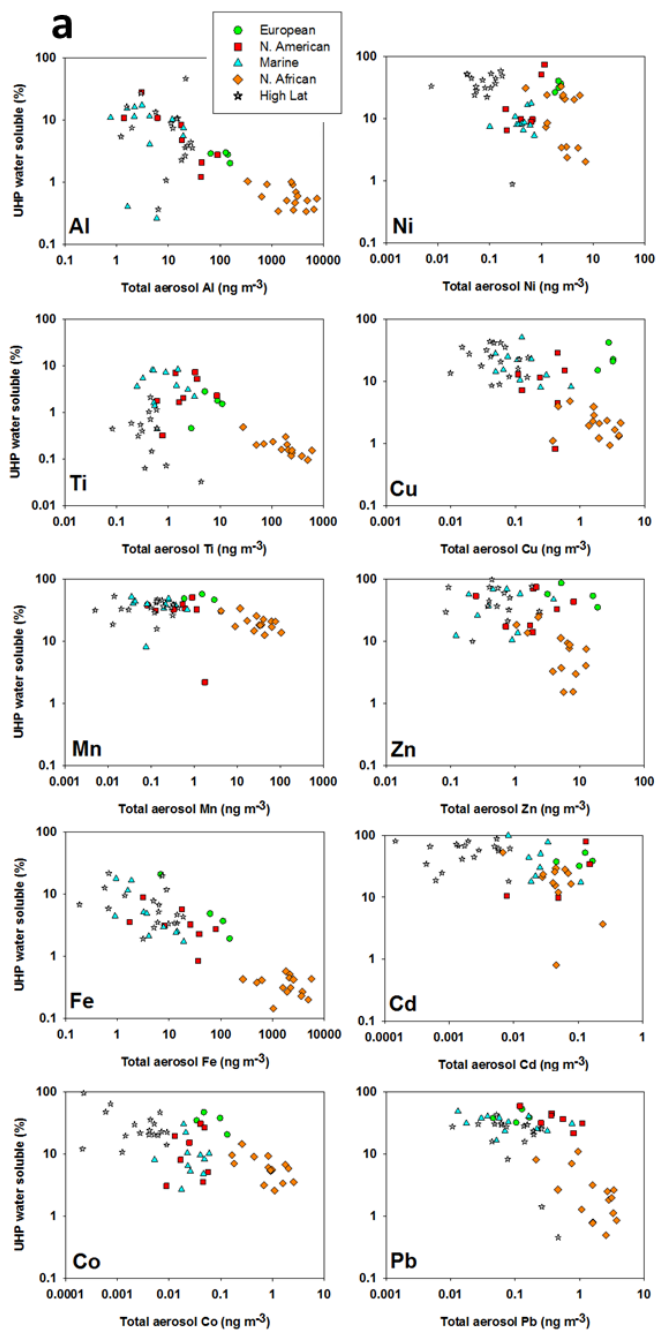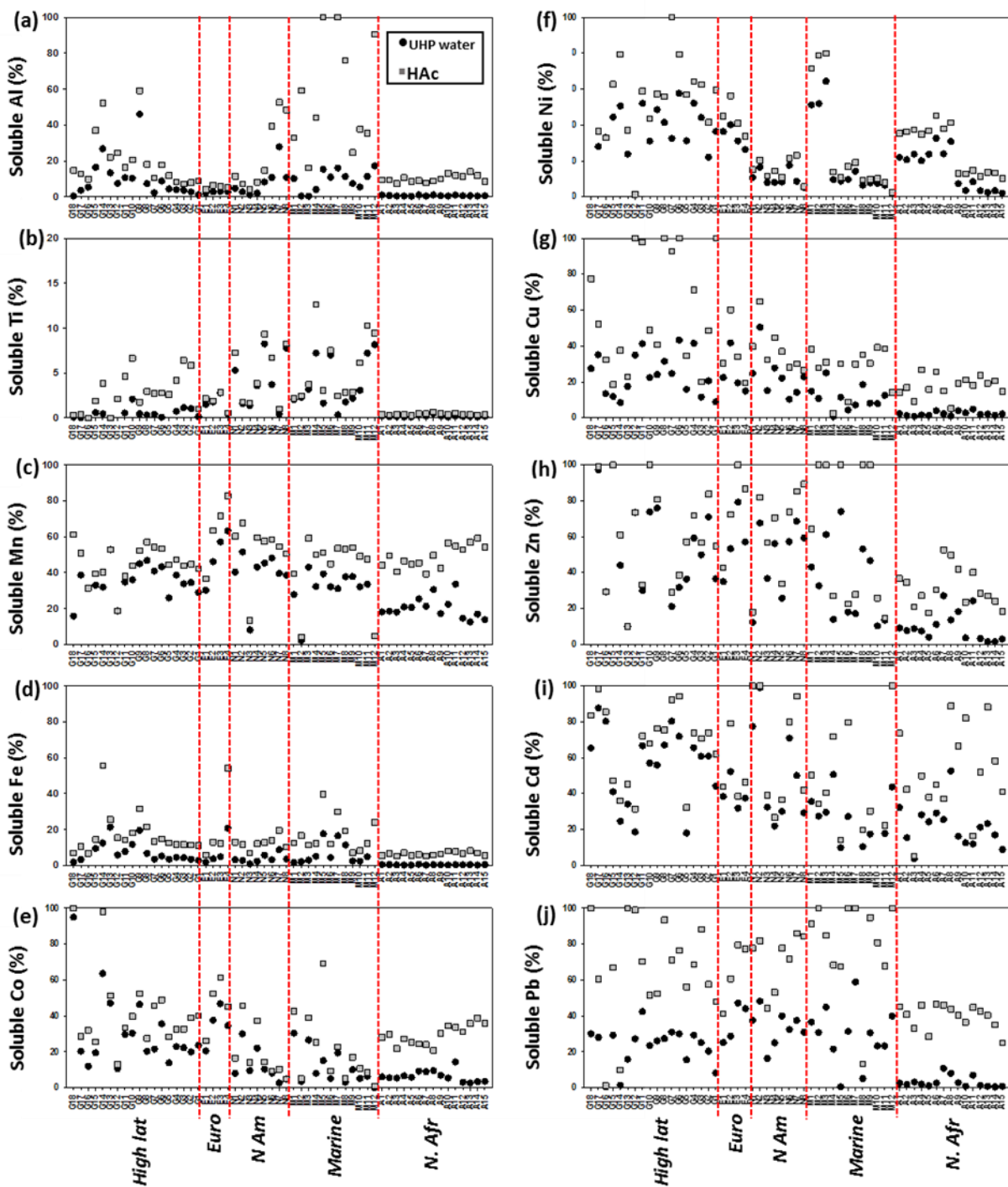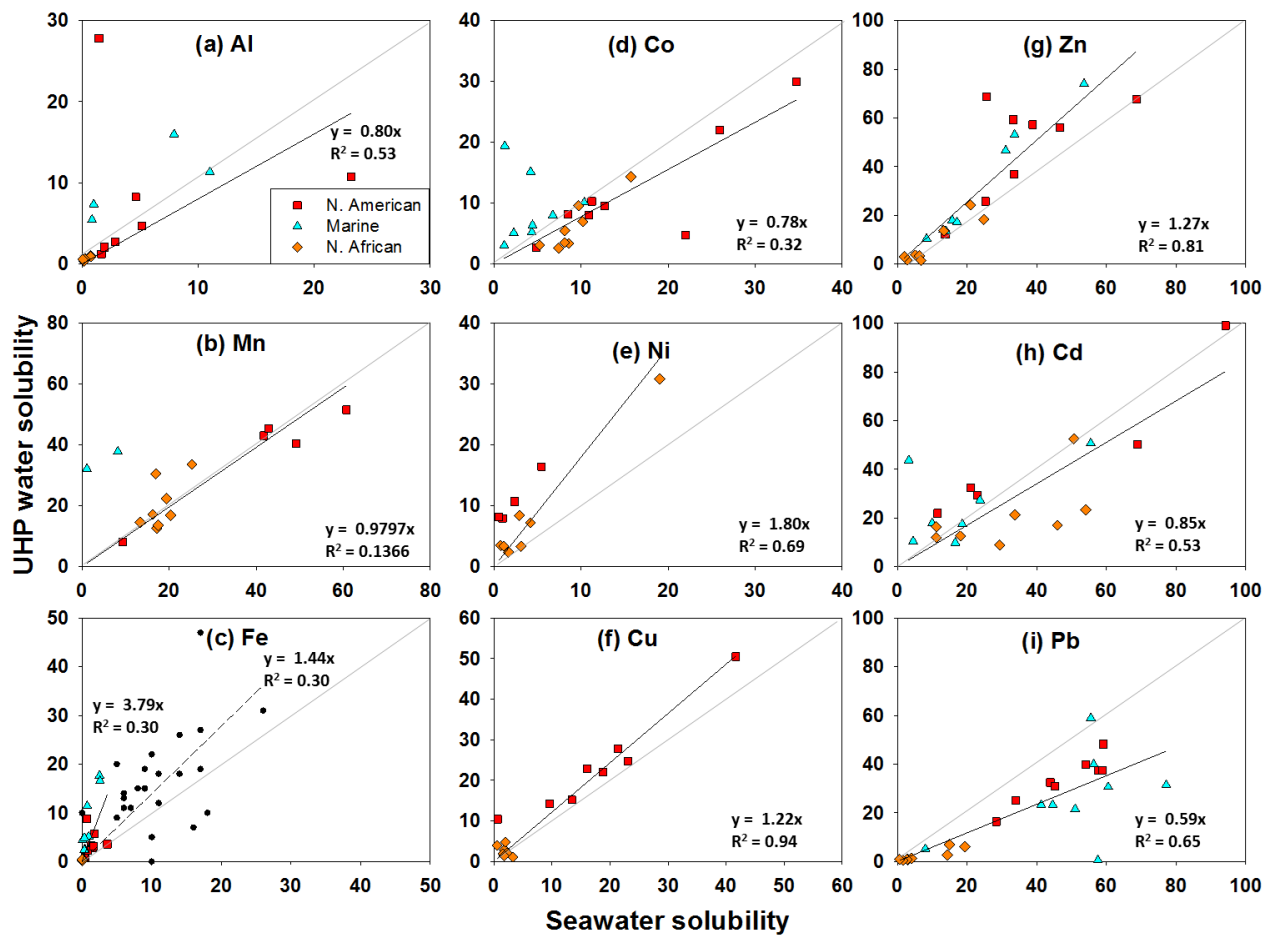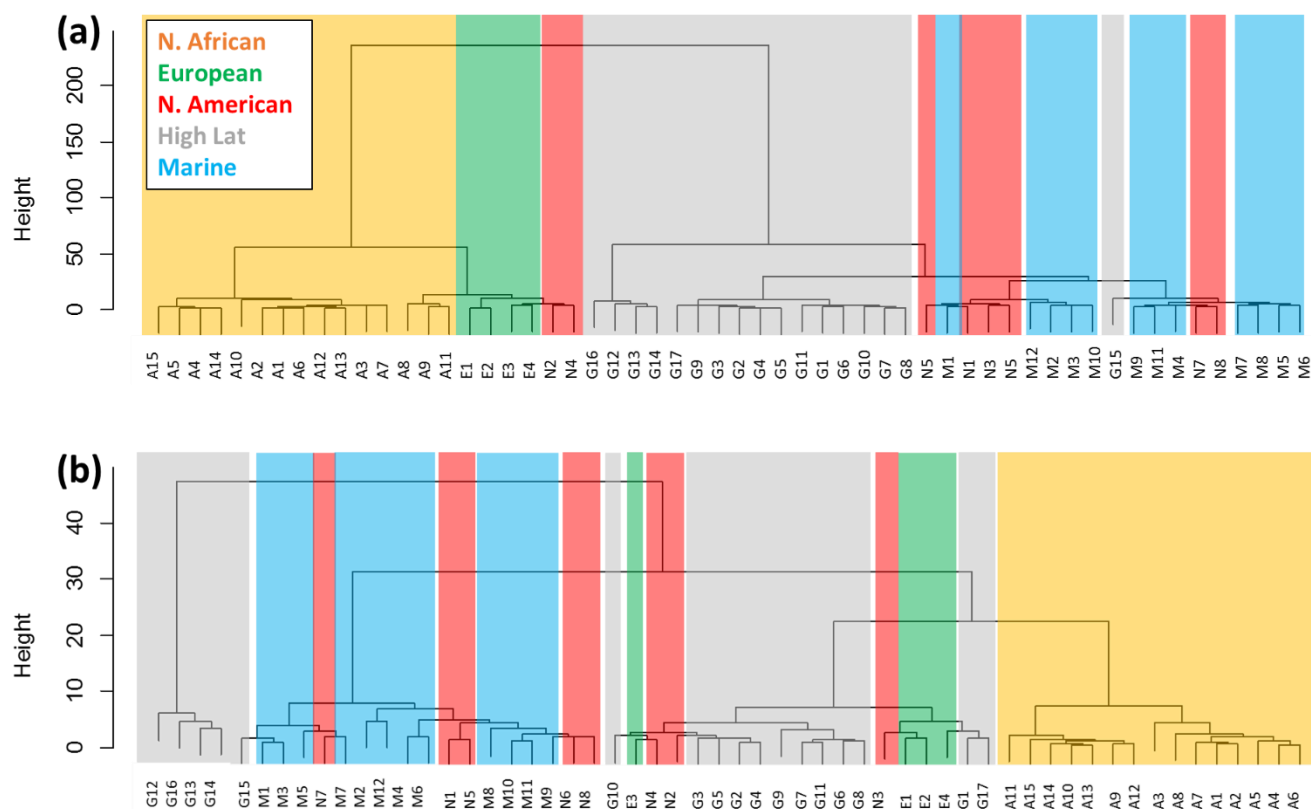
976 **Captions: Figures**
977
978 Figure 1. The GEOTRACES GA01 and GA03 cruise tracks (GA01, GA03-2010 and GA03-2011). In total, 57
979 aerosol samples (GA01 n = 18, GA03 n = 39; black dots) were collected. The samples are grouped by aerosol
980 source region (green = European (E1-4), blue = Marine (M1-12), yellow = North African (A1-15), red = North
981 American (N1-8), and grey = High Latitude (G1-18)), identified from air mass back trajectory simulations using
982 the NOAA ARL model, HYSPLIT (Stein et al., 2015; Rolph, 2017). Note that a different labelling convention
983 was used in Shelley et al. (2017) to refer to the GA01 samples. Here we use G1-18 to refer to the samples
984 collected during GA01 (A1-18 in Shelley et al., 2017), and A1-15 to refer to the North African samples from
985 GA03.
986
987 Figure 2. Total aerosol Fe and Al (ng m^{-3}) for: (a) all aerosol samples from cruises GA01 and GA03, (b)
988 samples from sources other than North Africa (i.e. the black diamonds in Fig. 2a), and (c) the samples inside the
989 dashed box in Fig. 2b. For High Latitude dust n = 18, European samples n = 4, North American samples n = 8,
990 Marine samples n = 12, and Saharan samples n = 15. Note error bars (standard deviations shown in Table S1)
991 are not included so as not to obscure the symbols.
992
993 Figure 3. Elemental mass ratios (normalised to Al) of total (black circles) and UHP water soluble (white
994 triangles) TEs. The UCC elemental ratio (Rudnick and Gao, 2003) is indicated by the solid horizontal line, and
995 the elemental ratio in North African sourced aerosols (Shelley et al., 2015) is indicated by the dashed horizontal

996   line on each plot. The red vertical lines separate the aerosol source regions, which are labelled in panel (a).
997   Samples G9-GA01 and M3-GA03 are indicated by blue arrows in panel c (see text for details).
998
999   Figure 4. (a) Percentage of UHP water soluble TE (calculated from Eq. 1) versus total aerosol TE (ng m^{-3}), (b)
1000 percentage of 25 % acetic acid soluble TE (calculated from Eq. 2) versus total aerosol TE (ng m^{-3}). Data is
1001 plotted on log-log scales.
1002
1003 Figure 5. Solubility of Al, Ti, Mn, Fe, Co, Ni, Cu, Zn, Cd, Pb following a UHP water leach (UHP water, black
1004 circles, calculated using Eq. 1), and a sequential leach of 25 % acetic acid (HAc, grey squares, calculated using
1005 Eq. 2). The red vertical dashed lines represent the different aerosol source categories, as labelled in panel (b).
1006 Note that Ti (panel b) is highly insoluble and has a maximum value of <13%. The data for this figure is also
1007 presented in Fig. S4 as biplots of UHP water fractional solubility versus 25 % acetic acid fractional solubility.
1008
1009 Figure 6. Comparison of TE solubility following instantaneous leaches using UHP water or locally-collected,
1010 filtered seawater. The solid line is the 1:1 line. Where fewer data are observed, concentrations were below
1011 detection for one or both of the two leaches. The data for soluble aerosol Fe from within our study region from
1012 Buck et al. (2010) are plotted as black circles in panel (c).
1013
1014 Figure 7. Heirarchical cluster analysis of (a) log transformed total TE concentration data plus NO_3^-
1015 concentration data, and (b) log transformed fractional solubility following the two-step sequential leach
1016 (fractional solubility calculated using Eq. 2) plus NO_3^- concentration data. The coloured blocks correspond with
1017 the aerosol source regions shown in the legend (note that the North African samples correspond with the yellow
1018 blocks of colour).
1019
1020
1021
1022